CHALMERS
UNIVERSITY OF TECHNOLOGY

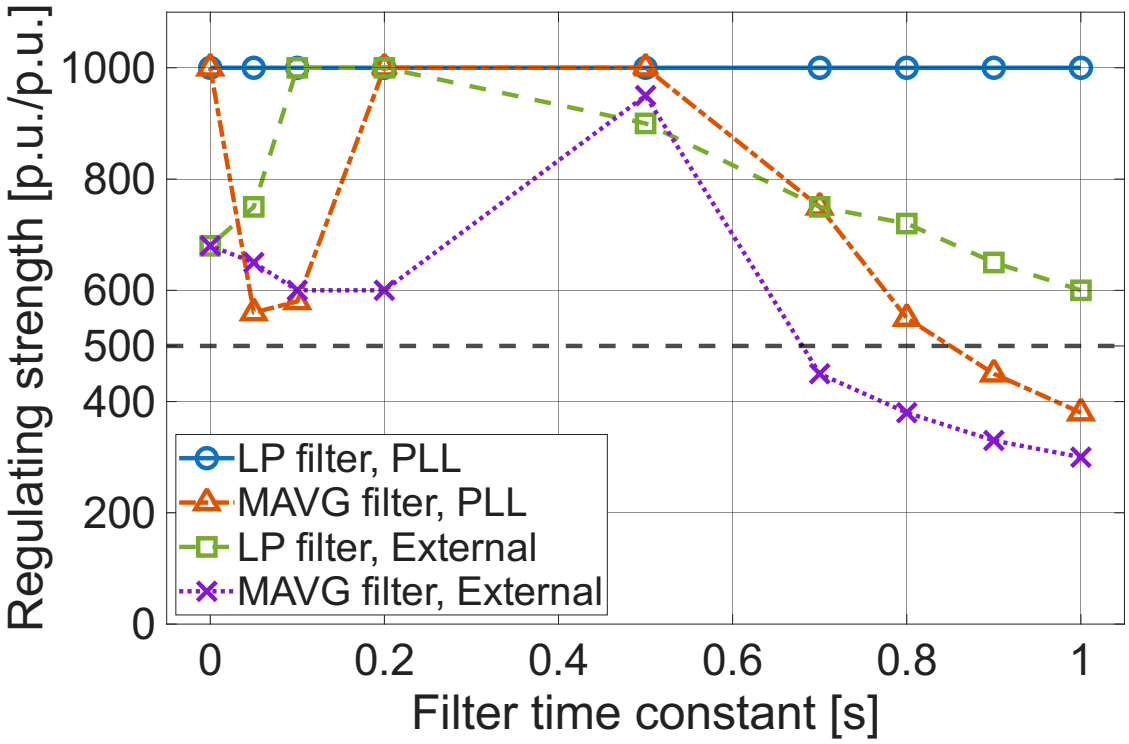

Stability of Frequency Regulation with a Grid Following Inverter

Master's thesis in Sustainable Electric Power Engineering and Electromobility

ANDRÉ EDVARDSSON
LILLY HAKESKOG

DEPARTMENT OF ELECTRICAL ENGINEERING
CHALMERS UNIVERSITY OF TECHNOLOGY
Gothenburg, Sweden 2026
www.chalmers.se

Master's thesis 2026

Stability of Frequency Regulation with a Grid Following Inverter

ANDRÉ EDVARDSSON
LILLY HAKESKOG

CHALMERS
UNIVERSITY OF TECHNOLOGY

Department of Electrical Engineering
Division of Electric Power Engineering
Chalmers University of Technology
Gothenburg, Sweden 2026

Stability of Frequency Regulation with a Grid Following Inverter
ANDRÉ EDVARDSSON, LILLY HAKESKOG

Supervisors: Bengt Johansson & Victor Lidskog, Solvina AB
Examiner: Peiyuan Chen, Department of Electrical Engineering

Master's Thesis 2026
Department of Electrical Engineering
Division of Electric Power Engineering
Chalmers University of Technology
SE-412 96 Gothenburg
Telephone +46 31 772 1000

Cover: Maximum achieved regulating strength indicating the stability limits for frequency regulation with a grid-following inverter operating in islanded mode, shown as a function of the frequency filters time constants. Further details are provided in Fig. 4.10a.

Typeset in LaTeX
Printed by Chalmers Reproservice
Gothenburg, Sweden 2026

Stability of Frequency Regulation with a Grid Following Inverter
ANDRÉ EDVARDSSON, LILLY HAKESKOG
Department of Electrical Engineering
Chalmers University of Technology

Abstract

With increasing integration of intermittent renewable generation, such as wind and solar power, additional frequency regulation is required in power systems. This is driven by generation fluctuations and reduced system inertia, as fossil fuel generation is phased out. Frequency regulation is partially provided through ancillary services, including frequency containment reserve for normal operation (FCR-N) and emerging services such as dynamic fast frequency reserve (dynamic FFR) and synthetic inertia, which aim to mitigate rapid frequency deviations. Most renewable energy sources are today connected through grid-following (GFL) inverters, which could provide these services. However, active power injection for frequency support can introduce local frequency disturbances that may destabilize the inverter. The stability of the inverter depends on the resulting frequency deviation, grid strength, and the inverter's frequency filter. This thesis investigates these stability challenges for a GFL inverter by evaluating the stability limits of regulating strength and synthetic inertia, as well as the performance of the frequency ancillary services at Chalmers University's power system laboratory.

The stability limits of FCR-N operation were evaluated both during grid-connected and islanded operation with a synchronous generator (SG), while synthetic inertia stability limits were assessed only during grid-connected operation. Grid strength was varied through changes in the impedance between the inverter and the local grid connection. The stability limits and performance of FCR-N, dynamic FFR, and synthetic inertia were investigated for different frequency measurement methods and frequency filters with varying time constants.

The results showed that a GFL inverter could provide frequency services while maintaining stable operation for most combinations of filters, filter time constants, and grid conditions, including islanded operation with an SG and grid-connected operation with varying grid impedance. Laboratory experiments demonstrated improved stability margins when a lead-lag filter was used to attenuate high-frequency components in the active power response. During islanded operation, the inverter could independently provide sufficient frequency regulation to maintain stable grid operation. For dynamic FFR, the inverter mitigated both the rate of change of frequency and the frequency nadir. Compared to synthetic inertia, dynamic FFR reduced the frequency nadir more effectively but required higher energy capacity for the same peak power output.

Keywords: grid-following inverter, frequency regulation, ancillary services, frequency containment reserve, FCR-N, dynamic FFR, synthetic inertia, island operation, grid strength, power system stability.

Acknowledgments

We would like to thank our supervisors Bengt Johansson and Victor Lidskog at Solvina AB. Your expertise, guidance and continuous support throughout this thesis work have been invaluable to us. Your engagement and enthusiasm made the entire process both educational, rewarding and enjoyable. We would also like to thank our examiner Peiyuan Chen for the guidance along the way and support in making the laboratory experiments possible.

Furthermore, we would like to express our gratitude to our colleagues at Solvina for making us feel very welcomed and supported during our thesis work. A special thanks goes to Christian Ekstrand for his valuable help in reviewing and providing feedback on our report.

André Edvardsson and Lilly Hakeskog, Gothenburg, June 2026

List of Acronyms

Below is the list of acronyms that have been used throughout this thesis listed in alphabetical order:

ENTSO-E	European Network of Transmission System Operators for Electricity
FCR	Frequency Containment Reserve
FCR-D	Frequency Containment Reserve for Disturbances
FCR-N	Frequency Containment Reserve for Normal Operation
FFR	Fast Frequency Reserve
GFL	Grid Following
GFM	Grid Forming
HP	High-Pass
LP	Low-Pass
MAVG	Moving Average
PC-DIV	Division-Based Power Controller
PC-PI	Proportional-Integral Based Power Controller
PI	Proportional-Integral
PLL	Phase-Locked Loop
POC	Point of Connection
RoCoF	Rate of Change of Frequency
SCR	Short-Circuit Ratio
SG	Synchronous Generator
SvK	Svenska Kraftnät
TSO	Transmission System Operator
VSC	Voltage Source Converter

Contents

List of Figures

List of Tables

1
Introduction

This chapter begins with a background on the thesis topic. Following this, the aim and limitations of the thesis are defined. The research questions that this thesis aims to solve are then presented.

1.1 Background

By the end of 2024, renewable energy sources reached 46% of installed power generation capacity in the world, leading to a growing share of the energy production from converter-based resources [1]. In contrast to synchronous generators in conventional power plants, converter-based sources do not naturally provide inertia to the energy system. If conventional units were to be phased-out, the power system would become more sensitive to frequency deviations due to lower system inertia.

During disturbances such as sudden loss of generation or load, the frequency of the grid deviates from its nominal value. To limit these deviations and restore frequency, frequency ancillary services are required [2]. Traditionally, these services were provided by conventional power plants such as coal, gas and hydro [3]. These generators also provide inertia, which slows the rate of change of frequency (RoCoF), following an imbalance in power [4].

An important frequency ancillary service is the frequency containment reserve (FCR), which acts to limit frequency deviations, within certain intervals. In the Nordic synchronous area FCR is divided into two categories, FCR for normal operation (FCR-N) and FCR for larger disturbances (FCR-D) [2]. As conventional generation is switched out for converter-based units, frequency ancillary services are therefore expected to be provided by converter-based units instead [3], such as wind power, photovoltaics, and battery energy storage systems. These services include established FCR and static fast frequency reserve (FFR) [2], as well as upcoming services under development including dynamic FFR and synthetic inertia. Frequency ancillary services will become more important in low inertia systems, where higher RoCoF reduces the available response time and drives the need for fast frequency response [4].

Most converter-based generation units today use grid-following (GFL) inverters [5]. These inverters rely on a separate unit generating the grid frequency and voltage waveform, typically a conventional synchronous generator or an stable and reliable

grid [3]. However, this dependency does not prevent GFL inverters from delivering various frequency ancillary services required to maintain a reliable grid. Grid-forming (GFM) inverters have been developed as an alternative that generates their own voltage and frequency references, regardless of the strength of the connected grid [3]. Although GFM inverters enhance system stability and are increasingly viewed as a key solution for future grids, their large-scale deployment is still evolving [6].

Improper tuning of control parameters in GFL inverters may lead to oscillations or slow dynamic response, which reduces overall system stability [7]. Consequently, technical requirements govern established services like FCR and static FFR prior to grid deployment [8]. These requirements are established by the European Network of Transmission System Operators for Electricity (ENTSO-E) and enforced by the transmission system operator (TSO) at the national level, such as Svenska Kraftnät (SvK) in Sweden. Therefore, compliance with these requirements must be demonstrated prior to connection and operation.

A real-world example of the evolving regulatory frameworks is Germany's new market for instantaneous reserve, launched in early 2026 [9]. This market enables converter-based energy sources to provide fast frequency response services such as synthetic inertia. Although these frameworks assume an increasing adoption of GFM inverters, it remains highly relevant to investigate the potential of more widely deployed GFL inverters for similar frequency services [5]. Therefore, this thesis also evaluates the capabilities of GFL inverters to provide fast frequency control. Previous work demonstrated the potential of both GFL and GFM inverters to provide frequency control in a simulated environment [10].

1.2 Aim

The aim of this master thesis is to investigate the stability limits and performance of frequency control implemented in a GFL inverter. In particular, the stability limits of FCR-N and synthetic inertia operations are evaluated, while the dynamic performance of FCR-N, dynamic FFR and synthetic inertia are analyzed under different grid conditions. Furthermore, the technical requirements for FCR-N specified by ENTSO-E are assessed. To improve stability and performance, the frequency measurement filters are analyzed and tuned. The power system laboratory at Chalmers will be used to evaluate the stability and performance of the GFL inverter.

1.3 Limitations

The evaluation of stability and performance for a GFL inverter is subject to several limitations associated with the laboratory setup and defined scope, which are presented in this section.

The inverter used in the laboratory is supplied directly from the local power grid and is modeled as an ideal source with unconstrained energy availability. This

assumption is made to isolate and evaluate the stability of the inverter control system independently of external generation or storage limitations. Therefore, the study does not consider the effects of finite energy availability or generation variability from renewable sources on stability and performance during frequency regulation experiments.

The investigation of different grid strengths is limited to strong, intermediate and weak grid conditions based on the available connections in the network model, which contains a limited number of π-sections. Furthermore, the voltage source with which the inverter operates is limited to the local power grid and a synchronous generator. An option would be to use a secondary inverter to emulate other types of grids or voltage sources, but the dynamics of introducing an additional inverter could have an unknown impact on the results. Studying the impact of a secondary emulating inverter is outside the scope of this study.

Since most converter-based generation units today utilize GFL technology [5], this thesis focuses on optimizing the functionality of GFL inverters. Therefore, GFM inverters are excluded from this study.

The testing of the GFL inverter with FCR functionality is limited to FCR-N, while FCR-D is not studied in this thesis. This scope is considered sufficient due to the similarities in their underlying control strategies. The primary differences between FCR-N and FCR-D lie in their operational frequency bands. Since FCR-N operates within a narrower frequency band (± 0.1 Hz) [11], it requires higher regulating strength. This higher gain increases the risk of control loop instability, making FCR-N more critical to evaluate.

1.4 Specification of the Issue Being Investigated

From the aim and limitations of this thesis project, this project intends to answer the following questions

Stability limits of a GFL inverter

- What are the stability limits that can be achieved with different frequency filters and frequency measurement methods?
- How does the strength of the grid affect the stability limits of the inverter?
- How does the stability limit of the inverter change between grid-connected and islanded operation?

Dynamic performance

- Can ENTSO-E's technical requirements be fulfilled for FCR-N?

- How could a GFL inverter support an SG in an islanded grid with frequency regulation?
- What similarities and differences are there between the performance of dynamic FFR and synthetic inertia for the evaluated GFL inverter?

Societal and ecological

- How do inverter-based technologies impact environmental emissions from electricity generation?
- What geopolitical challenges could arise from the implementation of inverter-based resources inverters?
- How can the implementation of frequency ancillary services through inverter-based resources inverters help improve societal perception regarding the reliability of renewable energy?
- How does the integration of digitally controlled inverters affect grid cybersecurity and system stability?

2

Modeling of Grid Following Inverter for Frequency Regulation

In this chapter, the mathematical models and control principles for grid-following inverter are presented. The chapter begins by establishing the fundamentals of the inverter and their role in providing different types of frequency ancillary services to the grid. This includes frequency containment reserve for normal condition (FCR-N), dynamic fast frequency reserve (dynamic FFR) and synthetic inertia. Thereafter, control architecture of the inverter is explained, after which the technical requirements for FCR-N are outlined. Currently, no technical requirements have been established for the other frequency ancillary services presented.

2.1 Grid Following Inverter Fundamentals

In a physical three-phase inverter, six insulated gate bipolar transistor (IGBT) switches are typically used to build a full bridge configuration [12]. A pulse width modulation (PWM) is often used to control these switches so that the inverter can synchronize its voltage and frequency to the grid. Since the focus in this thesis is on dynamics of the control loops, the timescale is in milliseconds to seconds. Switching dynamics in microseconds are therefore not as relevant and the high frequency harmonics that can be generated from the switches will not be considered. Consequently, assuming the inverter's output being well filtered, the six IGBT switches and PWM logic can be replaced by a controllable voltage source that represents the average output voltage for a switching period [13]. Therefore, the voltage source converter (VSC) in Fig. 2.1 is modeled as an average controllable voltage source.

The VSC's output voltage is driven by the signals from the control system's reference voltage magnitude $V_{\text{mag}}^{\text{ref}}$, phase angle $V_{\text{ang}}^{\text{ref}}$ and frequency f_{PLL}. In a GFL inverter, the voltage and current are measured at the point of connection (POC). Fig. 2.1 shows that the POC is the connection point between the inverter and the grid. The measured voltages are fed into a Phase-Locked Loop (PLL) where the frequency (f_{PLL}) and phase angle ($V_{\text{ang}}^{\text{ref}}$) are estimated [5]. The frequency is used in another controller to determine a power reference. The power reference is used in the power controller to calculate the current reference for the inverter, which the current controller then uses to calculate the voltage magnitude and phase reference.

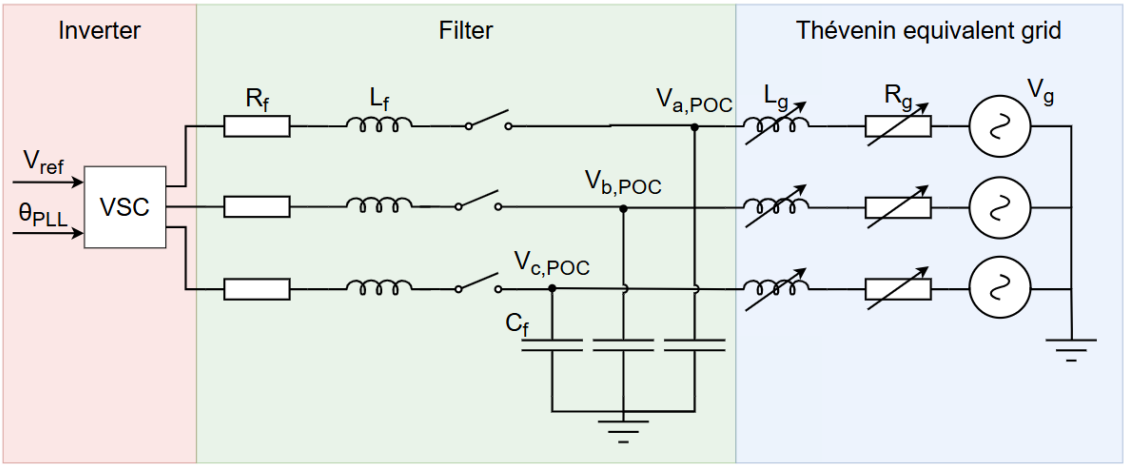

Figure 2.1: Circuit of the inverter together with its filter and the Thévenin equivalent grid.

The inverter is connected to the grid through a filter with resistance (R_f), inductance (L_f) and capacitance (C_f), as seen in Fig. 2.1. The filter is used to reduce harmonics or other transients that originate from the converter at the POC. At the POC, the grid is represented by a Thévenin equivalent, which models the power system as an ideal AC voltage source (V_g) behind a variable series impedance (R_g, L_g). A circuit breaker is placed between the inverter and the Thévenin equivalent grid to enable connection and disconnection.

To be able to investigate how a weak or strong grid affects the stability of the controllers in the inverter, the short-circuit ratio (SCR)

$$SCR = \frac{V_\mathrm{B}^2}{S_\mathrm{B} Z_\mathrm{sc}} \tag{2.1}$$

is used. In (2.1), V_B is the base voltage of the system, S_B is the apparent base power and Z_sc is the short-circuit impedance of the Thévenin equivalent grid. The short-circuit ratio is defined as the apparent short-circuit power in the POC divided by the rated power of the inverter [14]. A higher SCR indicates a stronger grid, which means reduced sensitivity to voltage dips during faults. Generally, a grid is classified as weak when the SCR is below 6 to 10, whereas values above 20 represents an exceptionally strong grid [14]. For this high SCR values, the grid behaves as a stiff voltage source and can therefore be approximated as an ideal source.

If the grid is weak, as described earlier, then the current that the inverter is supplying will heavily affect the voltage at the connection point and since that voltage is used in the PLL to estimate frequency and phase, this creates a feedback loop that can make the inverter unstable [3]. This limitation motivates the alternative use of GFM inverters, which act as voltage sources to eliminate the dependency on the grid strength. However, as many systems currently utilize GFL control, analyzing the PLL instability under weak grids remains relevant.

Since a GFL inverter is controlled digitally, the calculations are performed in discrete time. While the controller and inverter model are initially derived in the continuous domain, they must be discretized for digital hardware implementation. The discretization of continuous-time integral terms are achieved by the relation

$$\frac{1}{s} = \frac{T_\mathrm{s}}{z-1}, \tag{2.2}$$

where T_s is the sampling time, and z is the z-transform variable [15]. For the derivative, s, it is discretized by also assuming the derivative to be constant over a time step. Thus the derivative is found by taken the difference between the current and previous value, divided by the sampling time [16], which results in

$$s = \frac{1-\frac{1}{z}}{T_\mathrm{s}} = \frac{z-1}{zT_\mathrm{s}}. \tag{2.3}$$

The previous value is found by taking the unit delay, $1/z$, of the signal [15].

2.2 Frequency Ancillary Services in the Grid

The frequency of the grid is measured and sent to a control system which determines the desired power output. The implementation of the power regulation is determined by the type of frequency ancillary service. Three types of frequency ancillary services are studied in this thesis, FCR-N, dynamic FFR and synthetic inertia.

2.2.1 Frequency Containment Reserve

Within the Nordic synchronous area (consisting of Sweden, Norway, Finland, and Eastern Denmark), FCR is divided into two categories, normal and disturbance FCR [2]. The primarily difference between these two is the frequency interval in which they operate. While FCR-N operates within the 49.9-50.1 Hz range, which is considered normal condition of the grid [2], FCR-D operates within 49.5 - 50.5 Hz range, excluding the FCR-N interval. Apart from operating in different frequency intervals, both systems share the same proportional control principle. The reference output power for FCR is determined by

$$P_\mathrm{FCR,ref} = (f_\mathrm{ref} - f_\mathrm{PLL})K. \tag{2.4}$$

The output power is calculated from the deviation in the frequency, which is the difference between the reference frequency (f_ref) and the measured frequency (f_PLL) [17]. Lastly, the frequency deviation is scaled with the regulating strength,

$$K = \frac{1}{R} = \frac{\Delta P}{\Delta f} \tag{2.5}$$

where R is the droop factor. ΔP and Δf are the deviations in active power (MW) and frequency (Hz), respectively, so the unit of K in (2.5) is in MW/Hz. However, the regulating strength is usually scaled to p.u./p.u. by the base power and the base frequency. To dimension the FCR-N's regulating strength, a power interval is reserved within the unit's power capacity. The regulating strength is set to ensure full activation of the reserved capacity during the largest disturbance, for FCR-N being 0.1 Hz.

The implementation of FCR-N controller is presented in Fig. 2.2 and follows the relation in (2.4).

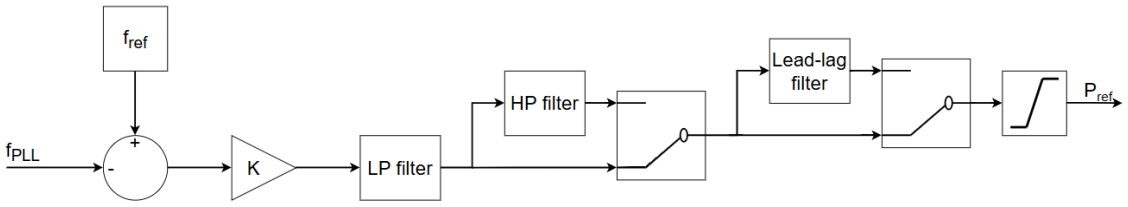

Figure 2.2: Block diagram of the frequency response controller. The lower path represents the FCR-N control, while the first selector switch activates the HP filter to provide dynamic FFR control. The second selector switch allows the lead-lag filter to be enabled for either FCR-N or dynamic FFR mode.

The FCR-N controller in Fig. 2.2 is equipped with a low-pass (LP) filter to attenuate transients and noise from frequency. Thus, the LP filter determines the regulator's sensitivity to frequency changes.

2.2.2 Dynamic Fast Frequency Reserve

The purpose of FFR is to counteract the initial fast and severe frequency deviations [18]. In contrast to FCR-N which aims to regulate the frequency to a steady-state level, FFR aims to reduce the RoCoF and the nadir/zenith. Hence, FFR do not regulate the frequency to achieve a steady-state level.

FFR is divided into static and dynamic FFR. The static FFR is already an established service for the Nordic TSO:s. Static FFR is designed after its activation frequency, at which maximum power is to be delivered within a certain time frame [19]. Static FFR does not have any regulation of its power output and is at maximum power throughout the duration of support. After supporting, it can ramp down and start to recover [19].

However, dynamic FFR can regulate its power output after the frequency deviation. The implementation is done following the FCR controller, but adding a high-pass (HP) filter to the output signal [20]. The HP filter in cascade with the LP filter creates a band-pass filter, that allows transients and fast frequency changes to pass through. The block diagram can be seen in Fig. 2.2 by connecting the HP filter.

2.2.3 Synthetic Inertia

The inertia in the system determines how sensitive the grid frequency is to active power disturbances. In hydro, nuclear and thermal plants the generators are rotating with the grid frequency, thus for the grid frequency to change the generators has to change their frequency as well [21]. This need to change the generators frequency yields an inertia in the system. The relation between the RoCoF and a power disturbance is described by the swing equation [22],

$$\frac{2H}{f_{\mathrm{n}}}\frac{df}{dt} = P_{\mathrm{m}} - P_{\mathrm{e}}, \tag{2.6}$$

where H is the inertia constant, f_{n} is the nominal frequency, $\frac{df}{dt}$ is the RoCoF, P_{m} and P_{e} is the mechanical respective the electric power.

Unlike traditional generators, inverter-based units do not inherently provide inertia since they consist of only power electronics and therefore lack a synchronously coupled rotating mass [23]. However, the control system could be adapted to emulate inertia. The equation to derive the controller for synthetic inertia is found by first deriving the swing equation in per-unit as

$$2H\frac{df_{\mathrm{pu}}}{dt} = P_{\mathrm{m,pu}} - P_{\mathrm{e,pu}}, \tag{2.7}$$

where all variables are expressed in per-unit except for the inertia constant H, which remians in seconds [23]. Since inverters has no mechanical power, $P_{\mathrm{m,pu}}$ is set to zero. Then extracting the electrical power from (2.7) the output power of the inverter is found as

$$P_{\mathrm{e,pu}} = -2H\frac{df_{\mathrm{pu}}}{dt}. \tag{2.8}$$

2.3 *dq*-Frame

The power system consists of three phases, where each phase ideally has the same amplitude but phase shifted 120° from each other. The power system could thus be expressed by three references axes spaced 120° apart. Then along its respective references axis the electric quantity for phase a, b or c is represented. Each electric quantity is time varying quantity which moves along its reference axis. Since, the reference axis are not independent from each-other, each electric quantity can be projected onto a 2-axis reference system. The new reference system is referred to as the $\alpha\beta$ coordinate system, where the α axis is aligned along the a axis, while the β axis is shifted 90° lagging [24]. There are two variants of Clarke transformation to project from abc to $\alpha\beta$. Power-invariant transformation has a scaling factor of $\sqrt{\frac{2}{3}}$ and amplitude invariant transformation

$$\begin{bmatrix} \alpha \\ \beta \end{bmatrix} = \frac{2}{3} \begin{bmatrix} 1 & -\frac{1}{2} & -\frac{1}{2} \\ 0 & \frac{\sqrt{3}}{2} & -\frac{\sqrt{3}}{2} \end{bmatrix} \begin{bmatrix} a \\ b \\ c \end{bmatrix}, \tag{2.9}$$

has a scaling factor of $\frac{2}{3}$. Using the amplitude-invariant transformation in (2.9), the amplitude in $\alpha\beta$ coordinates is the same as in *abc*. However, when calculating the power in $\alpha\beta$ a scaling factor is needed. On the other hand, the power in $\alpha\beta$ and *abc* is equal when using power-invariant transformation, but it causes the amplitudes to be scaled incorrectly.

Similar to the *abc* reference frame, quantities in the $\alpha\beta$ frame still varies with grid frequency. Therefore, instead of the quantities varying, the reference-frame is rotated synchronously with the grid, making the phase quantities being stationary. With the $\alpha\beta$ coordinates determined in (2.9) the new rotating reference frame (dq) is found with the Park transformation [24], by

$$\begin{bmatrix} d \\ q \end{bmatrix} = \begin{bmatrix} \cos\theta & -\sin\theta \\ \sin\theta & \cos\theta \end{bmatrix} \begin{bmatrix} \alpha \\ \beta \end{bmatrix}, \tag{2.10}$$

where θ corresponds to the phase angle of the power system. The properties of the selected Clarke transformation are transferred to the Park transformation.

A transformation matrix T^{dq} is derived to map the cartesian system directly onto to dq frame. The transformation matrix is found by multiplying (2.9) with (2.10), which results in the matrix

$$T^{\mathrm{dq}} = \frac{2}{3} \begin{bmatrix} \cos\theta & -\sin(\theta + \frac{\pi}{6}) & -\sin(\frac{\pi}{6} - \theta) \\ \sin\theta & \cos(\theta + \frac{\pi}{6}) & -\cos(\frac{\pi}{6} - \theta) \end{bmatrix}. \tag{2.11}$$

2.4 Phase-Locked Loop

The phase angle θ in the Park transformation (2.10) cannot be directly measured, it must be estimated using for example a PLL. The aim of the PLL is to align the voltage vector with the d-axis in the dq-frame by measuring the angle between the d and q component [25]. To align the voltage with the d-axis, this angle should be zero. Consequently, the angle (δ) is treated as the estimation error, which the proportional-integral (PI) regulator uses to generate a new estimation as can be seen in Fig. 2.3.

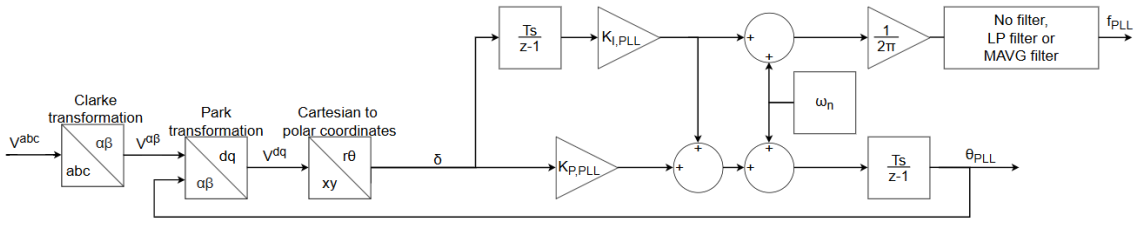

Figure 2.3: Block diagram of the PLL.

The nominal angular frequency is denoted with ω_{n} in Fig. 2.3. The PLL's PI controller outputs the deviation between the estimated angular frequency and the angular frequency measured from the grid frequency at the POC. This is then used to estimate the grid frequency (f_{PLL}) and phase angle (θ_{PLL}). The estimated phase angle is then fed back to the coordinate transformations for subsequent calculations. With the angle difference between d and q treated as the estimation error and Fig. 2.3, the transfer function of the PLL is

$$\theta_{\mathrm{PLL}} = \frac{1}{s}(\omega_{\mathrm{n}} + (K_{\mathrm{P,PLL}} + \frac{1}{s}K_{\mathrm{I,PLL}})\delta) \approx (\frac{1}{s}K_{\mathrm{P,PLL}} + \frac{1}{s^2}K_{\mathrm{I,PLL}})\delta. \tag{2.12}$$

The gains of the PI controller are defined as $K_{\mathrm{P,PLL}}$ and $K_{\mathrm{I,PLL}}$, which are the proportional and integral gain, respectively. From (2.12) the transfer function is derived, and its denominator is set equal to a second-order LP filter, due to the two poles from the PI integrator and the phase angle integrator. The transfer function is thus

$$\frac{\theta_{\mathrm{PLL}}}{\delta} = \frac{K_{\mathrm{I,PLL}} + sK_{\mathrm{P,PLL}}}{s^2 + sK_{\mathrm{P,PLL}} + K_{\mathrm{I,PLL}}}. \tag{2.13}$$

As seen in (2.13), the denominator of the transfer function is of the same order as a second-order LP filter. Thus, setting the denominator of the transfer function equal to the denominator of a second-order LP filter gives

$$s^2 + sK_{\mathrm{P,PLL}} + K_{\mathrm{I,PLL}} = s^2 + 2 \cdot 2\pi f_{\mathrm{PLL}}\zeta s + 2\pi f_{\mathrm{PLL}}, \tag{2.14}$$

where f_{PLL} is the desired bandwidth [Hz] of the PLL and ζ is its damping factor. From Fig. 2.3, it can be seen that the frequency is extracted from the integrator, excluding the proportional gain ($K_{\mathrm{P,PLL}}$). This is because the proportional gain is sensitive to phase jumps (high frequency dynamics), whereas the integrator is not. This results in more stable and accurate frequency measurements. Furthermore, the estimated frequency (f_{PLL}) in Fig. 2.14 can be used unfiltered, filtered through an LP filter or a moving average (MAVG) filter. The types of filters used are described in Section 2.8.

2.5 Power Controller

Given the reference power (P_{ref}) from the FCR controller, the power controller calculates a corresponding reference current ($I^{\mathrm{d}}_{\mathrm{ref}}$). Two types of power controllers are introduced, a proportional-integral based (PC-PI) and a simplified power controller with division-based calculation (PC-DIV).

2.5.1 Proportional-Integral Based Power Controller

Since apparent power is the combination of active and reactive power, two separate PI-integrators are used, seen in Fig. 2.4. The active power controller, calculates the active current component, I_{P}, which is equal to the d-axis current, $I_{\mathrm{ref}}^{\mathrm{d}}$ [17]. Moreover, the reactive power controller determines the reactive current, I_{Q}, which has a different polarity from $I_{\mathrm{ref}}^{\mathrm{q}}$.

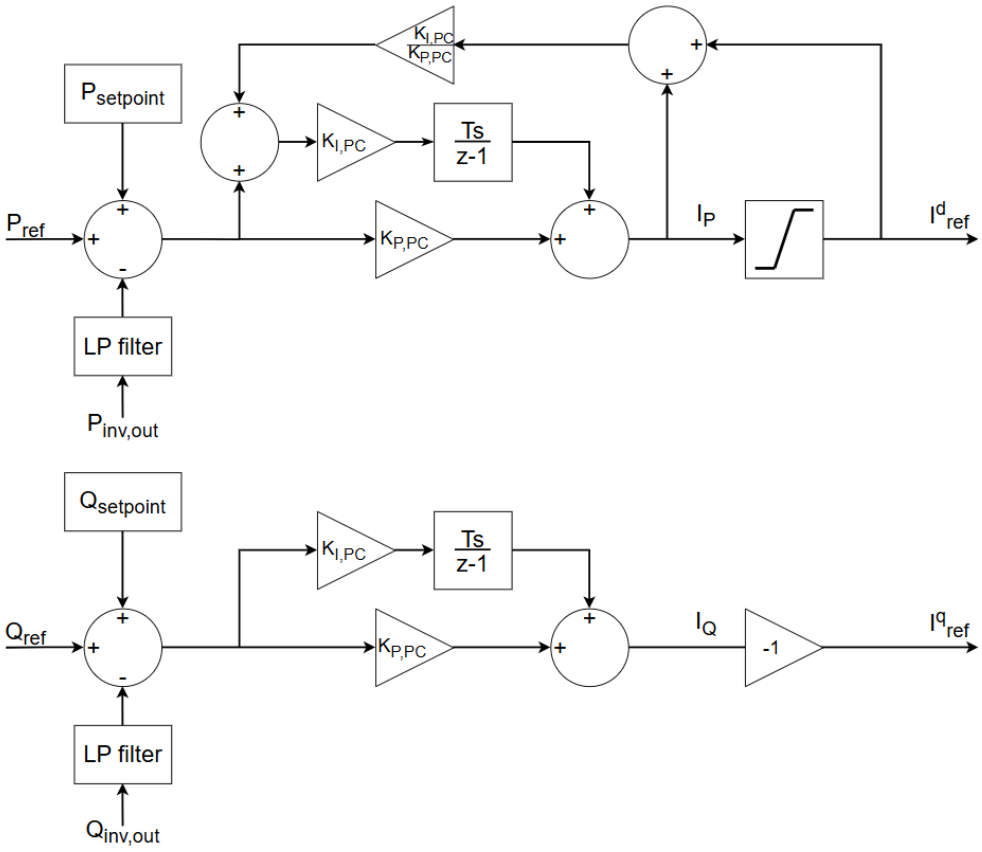

Figure 2.4: Block diagram of the PC-PI.

The PI-regulator compensates for the error between the measured active power ($P_{\mathrm{inv,out}}$) and the total active power demand. The total active power demand is the sum of the active power reference (P_{ref}) from the frequency controller and the active power setpoint (P_{setpoint}). For reactive power, the error is calculated by the difference between the reference (Q_{ref}), setpoint (Q_{setpoint}) and measured ($Q_{\mathrm{inv,out}}$), where the reference is set to zero if no reactive power regulation is implemented.

The proportional ($K_{\mathrm{P,PC}}$) and integral ($K_{\mathrm{I,PC}}$) gains in Fig. 2.4 is tuned until the desired time constant is achieved for a power step in P_{ref}. The tuned parameters are found in Section 3.4.2.

Furthermore, the active power regulator is equipped with an anti-windup. This is necessary since the integrator would otherwise be prone to integral-windup due to the active power reference not being limited, while the inverter output being limited

by its power rating. The limitations of the inverter are symmetric with the rated power, meaning $P_{\text{min}} = -P_{\text{max}}$. Meanwhile, it is not needed in the reactive power controller if the reference is set to zero and assuming small variations in the produced reactive power.

2.5.2 Simplified Power Controller with Division-Based Calculation

An alternative to traditional PI-based control is the division-based power controller. This approach incorporates two simplifications of the PI-controller. Firstly, since no reactive power regulation is implemented and assume that the active power has negligible influence on the produced reactive power, the reactive power controller is removed. Instead of a controller, the current, $I^{\text{q}}_{\text{ref}}$, reference is set to zero.

Secondly, the mathematical relation between active power and I^{d} is utilized, which replaces the active power PI-integrator. The voltage at the POC is assumed to be aligned with the d-axis, $V_{\text{POC}} = V^{\text{d}}_{\text{POC}}$, as for the PLL derivation. The reference apparent power at the POC is calculated as

$$S_{\text{ref}} = V^{\text{dq}}_{\text{POC}} I^{\text{dq}*}_{\text{ref}} = V^{\text{d}}_{\text{POC}}(I^{\text{d}}_{\text{ref}} - jI^{\text{q}}_{\text{ref}}) = V^{\text{d}}_{\text{POC}} I^{\text{d}}_{\text{ref}} - jV^{\text{d}}_{\text{POC}} I^{\text{q}}_{\text{ref}}, \tag{2.15}$$

where $I^{\text{dq}}_{\text{ref}}$ is the reference current of the inverter. The real part in (2.15) equals the active power reference of the inverter. Hence, the active current relation with the active power is found as

$$I^{\text{d}}_{\text{ref}} = \frac{P_{\text{ref}}}{V^{\text{d}}_{\text{POC}}} = \frac{P_{\text{ref}}}{|V_{\text{POC}}|}. \tag{2.16}$$

With the assumption that the voltage was aligned with the d-axis, (2.16) is simplified to only consider the magnitude of the POC voltage. The implementation of this power controller is shown in Fig. 2.5.

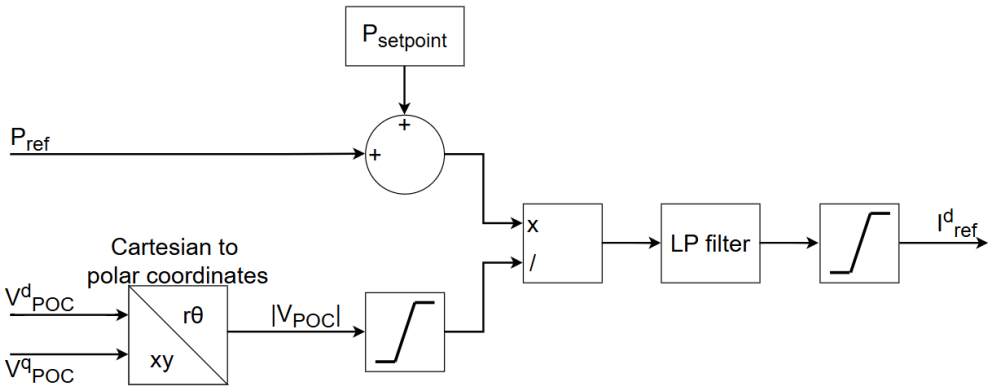

Figure 2.5: Block diagram of the PC-DIV.

The direct calculation from the PC-DIV offers a direct response but has two drawbacks. As the POC voltage approaches zero, the reference current tends towards infinity, which can be solved by setting limitations on $|V_{\mathrm{POC}}|$. The reference current is also limited and the chosen settings are detailed in Section 3.5.1. Furthermore, the absence of an integration term results in a controller that is unable to eliminate its steady-state errors in the power produced.

2.6 Current Controller

The purpose of the current controller is to regulate the inverter's output voltage to ensure that the output current matches the reference current. To achieve this, the closed-loop transfer function,

$$H(s) = \frac{F(s)G(s)}{F(s)G(s)+1} = \frac{2\pi f_{\mathrm{CC}}}{s+2\pi f_{\mathrm{CC}}}, \tag{2.17}$$

of the current controller and the filter is modeled as a first-order LP filter [26], with a bandwidth of f_{CC}. To find the current controller function $F(s)$, the filter function $G(s)$ must first be defined. Applying Kirchhoff's voltage law on the filter presented in Fig. 2.1 and assuming current going out of the inverter, the terminal voltage is

$$V_{\mathrm{inv}} = V_{\mathrm{POC}} + R_{\mathrm{f}} I + L_{\mathrm{f}} \frac{dI}{dt}. \tag{2.18}$$

where V_{POC} is the voltage at the POC. The system in (2.18) is defined with physical dimensions. To simplify further calculations, (2.18) is converted into per-units. This is done by dividing the whole expression with the base voltage, V_{B}, thus (2.18) becomes

$$\frac{V_{\mathrm{inv}}}{V_{\mathrm{B}}} = V_{\mathrm{pu,inv}} = \frac{V_{\mathrm{POC}}}{V_{\mathrm{B}}} + \frac{R_{\mathrm{f}} I}{R_{\mathrm{B}} I_{\mathrm{B}}} + \frac{L_{\mathrm{f}} \frac{dI}{dt}}{\omega_{\mathrm{B}} L_{\mathrm{B}} I_{\mathrm{B}}} = V_{\mathrm{pu,POC}} + R_{\mathrm{pu,f}} I_{\mathrm{pu}} + \frac{L_{\mathrm{pu,f}}}{\omega_{\mathrm{B}}} \frac{dI_{\mathrm{pu}}}{dt}, \tag{2.19}$$

where R_{B}, L_{B}, ω_{B} and I_{B} is its respective base values. With the parameters in p.u. the transformation to dq frame is carried out. To transform (2.19) into dq, the transformation matrix T^{dq} defined in (2.11), is applied. The terminal voltage in p.u. is

$$T^{\mathrm{dq}} V_{\mathrm{pu,inv}} = T^{\mathrm{dq}} V_{\mathrm{pu,POC}} + R_{\mathrm{f}} T^{\mathrm{dq}} I_{\mathrm{pu}} + L_{\mathrm{pu,f}} \frac{dT^{\mathrm{dq}}}{dt} I_{\mathrm{pu}} + \frac{L_{\mathrm{pu,f}}}{\omega_{\mathrm{B}}} T^{\mathrm{dq}} \frac{dI_{\mathrm{pu}}}{dt}. \tag{2.20}$$

The transformation matrix T^{dq} is dependent on the time as seen in (2.11), since the phase angle is time dependent. Therefore, the product rule has to be applied

on (2.20) on both the transformation matrix and the current. Furthermore, the chain rule has also been applied on the transformation matrix, thus canceling ω_{B}. Thereafter (2.20) is converted into the Laplace domain,

$$T^{\mathrm{dq}}V_{\mathrm{pu,inv}}(s) = T^{\mathrm{dq}}V_{\mathrm{pu,POC}}(s) + R_{\mathrm{pu,f}}T^{\mathrm{dq}}I_{\mathrm{pu}}(s) + L_{\mathrm{pu,f}}\dot{T}_{\mathrm{dq}}I_{\mathrm{pu}}(s) + s\frac{L_{\mathrm{pu,f}}}{\omega_{\mathrm{B}}}T^{\mathrm{dq}}I_{\mathrm{pu}}(s). \tag{2.21}$$

The term with derivative of the transformation matrix in (2.20) introduces cross-coupling between the d- and q-currents [26]. Therefore, is the d and q components analyzed separately rather than collectively as shown in (2.21)

$$\begin{cases} V^{\mathrm{d}}_{\mathrm{pu,inv}} = V^{\mathrm{d}}_{\mathrm{pu,POC}}(s) + R_{\mathrm{pu,f}}I^{\mathrm{d}}_{\mathrm{pu}}(s) - L_{\mathrm{pu,f}}I^{\mathrm{q}}_{\mathrm{pu}}(s) + s\frac{L_{\mathrm{pu,f}}}{\omega_{\mathrm{B}}}I^{\mathrm{d}}_{\mathrm{pu}}(s) \\ V^{\mathrm{q}}_{\mathrm{pu,inv}} = V^{\mathrm{q}}_{\mathrm{pu,POC}}(s) + R_{\mathrm{pu,f}}I^{\mathrm{q}}_{\mathrm{pu}}(s) + L_{\mathrm{pu,f}}I^{\mathrm{d}}_{\mathrm{pu}}(s) + s\frac{L_{\mathrm{pu,f}}}{\omega_{\mathrm{B}}}I^{\mathrm{q}}_{\mathrm{pu}}(s). \end{cases} \tag{2.22}$$

In (2.22) the filter is defined, however there is a cross-coupling between $I^{\mathrm{d}}_{\mathrm{pu}}$ and $I^{\mathrm{q}}_{\mathrm{pu}}$, and the voltage at the POC creates a non-linearity. Since neither the cross-coupling nor V_{POC} contains a s or $1/s$ factor, and both are independent of the same d or q component, neither is directly controlled by the current controller. Hence, for the determination of the current controller, the cross-coupling and V_{POC} are momentarily removed. The transfer function of the filter becomes the following

$$G(s) = \frac{I^{\mathrm{dq}}_{\mathrm{pu}}(s)}{V^{\mathrm{dq}}_{\mathrm{pu,inv}}} = \frac{1}{R_{\mathrm{pu,f}} + s\frac{L_{\mathrm{pu,f}}}{\omega_{\mathrm{B}}}}. \tag{2.23}$$

Extracting the controller function, $F(s)$, from (2.17) and inserting the filter function (2.23), $F(s)$ is found to be

$$F(s) = \frac{2\pi f_{\mathrm{CC}}}{sG(s)} = 2\pi f_{\mathrm{CC}}\frac{L_{\mathrm{f}}}{\omega_{\mathrm{b}}} + 2\pi f_{\mathrm{CC}}\frac{R_{\mathrm{f}}}{s} = K_{\mathrm{P,CC}} + \frac{K_{\mathrm{I,CC}}}{s}. \tag{2.24}$$

After deriving the transfer function for the PI regulator, the cross-coupling and V_{POC} from (2.22) are reinstated. The corresponding block diagram for the current controller is presented in Fig. 2.6.

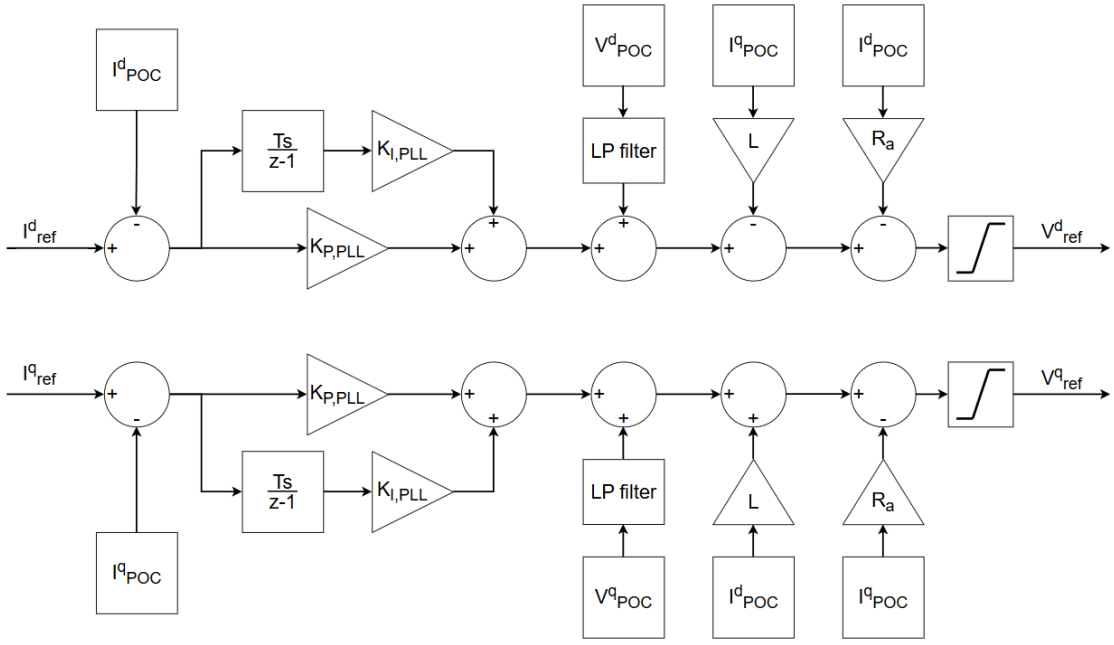

Figure 2.6: Block diagram of the current controller.

This current controller loop serves as the final component of the inverter's control structure, detailed in the following section.

2.7 Connection of Controllers

The overall control structure and the connections between different controllers are illustrated in Fig. 2.7. As shown, the system has a cascaded layout with the PLL that handles synchronization, allowing the power controller to generate the reference for the inner current controller loop. Then, the inverter's output is regulated by the current controller.

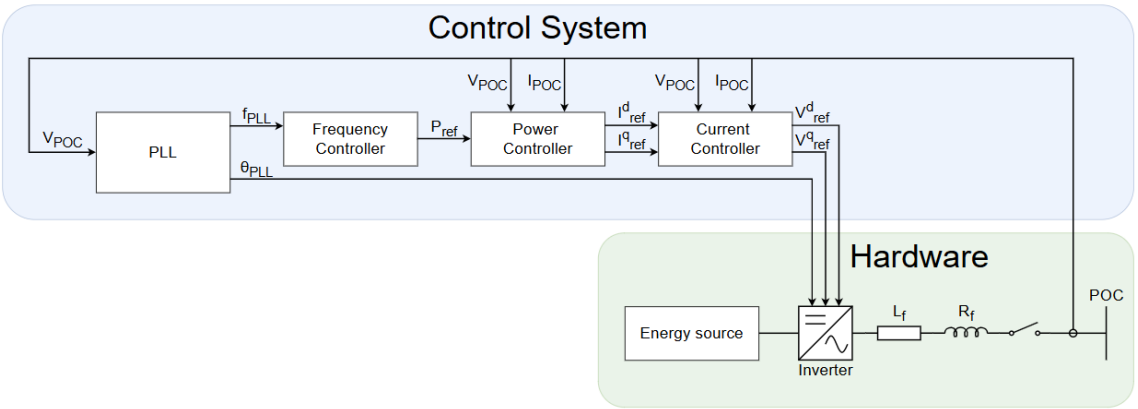

Figure 2.7: Overview of the control structure and connections between the controllers.

This cascaded layout creates a feedback loop where the inverter dynamics are coupled to the grid through the POC voltage, which is used by the PLL to estimate the grid frequency. The estimated frequency deviations drive a power response according to (2.4) and (2.8). This impacts the phase angle θ as can be seen by the two-port equation

$$P = \frac{V_{\mathrm{POC}} V_{\mathrm{g}}}{\omega L_{\mathrm{g}}} sin(\theta) = \frac{V_{\mathrm{POC}} V_{\mathrm{g}}}{\omega L_{\mathrm{g}}} sin(\theta_{\mathrm{POC}} - \theta_{\mathrm{g}}), \tag{2.25}$$

where θ_{POC} and θ_{g} are the phase angles at the POC and at the connection point of the voltage source V_{g} as seen in Fig. 2.1. The resistive component of the variable series impedance (R_{g}, L_{g}) is neglected since the inductive reactance of a transmission line typically dominates the resistance, making the X/R ratio large enough to assume a lossless line. For a strong voltage source, the θ_{g} can be treated as a stiff reference. Seen in (2.25), variations in transferred power lead to changes in θ_{POC}. A rate of change in θ_{POC} corresponds to a deviation in the local frequency as

$$f_{\mathrm{POC}} = \frac{1}{2\pi f_{\mathrm{B}}} \frac{d\theta_{\mathrm{POC}}}{dt}. \tag{2.26}$$

This frequency is measured by the PLL, which closes the loop. However, because the active power injected is dependent on the measured frequency ((2.4) and (2.8)) which in turn is affected by fast changes in P ((2.25) and (2.26)), there is a risk of instability.

The closed-loop instability is influenced mainly by three factors: the grid strength, the regulation gain of frequency controller and inverter's response time. The strength dependence of the grid is seen in (2.25), with a small L_{g} (indicating a stronger grid) the change of P resulting in a small change in θ_{POC}. The change in θ_{POC} also depends on the size of P, which is regulated by the gain of the frequency controller. For FCR-N and dynamic FFR the regulating strength corresponds to its controller gain, while for synthetic inertia it corresponds to the inertia constant. Lastly, from (2.26) it is seen that the rate of change affects the stability of the closed-loop, caused by the inverter's response and measurement. The inverter's response and measurement are therefore filtered.

2.8 Filtering Methods

In the controllers, the raw measured signals can often be noisy. This creates the need to filter the signal in order to provide clean and stable inputs and outputs for the different controllers. Two common types of filters for noise suppression are LP filter and moving average filter.

A LP filter suppresses frequencies over the cut-off frequency, ω_c, such as ripple or noise [27]. While lower frequencies, below the cut-off frequency, are unaffected. The first order LP filter is defined as

$$H(s) = \frac{\omega_c}{s + \omega_c}. \tag{2.27}$$

Fig. 2.8 shows the LP filter's frequency response. It demonstrates that a larger time constant ($\tau_{\text{LP}} = 1/\omega_c$) results in a lower bandwidth and more phase lag.

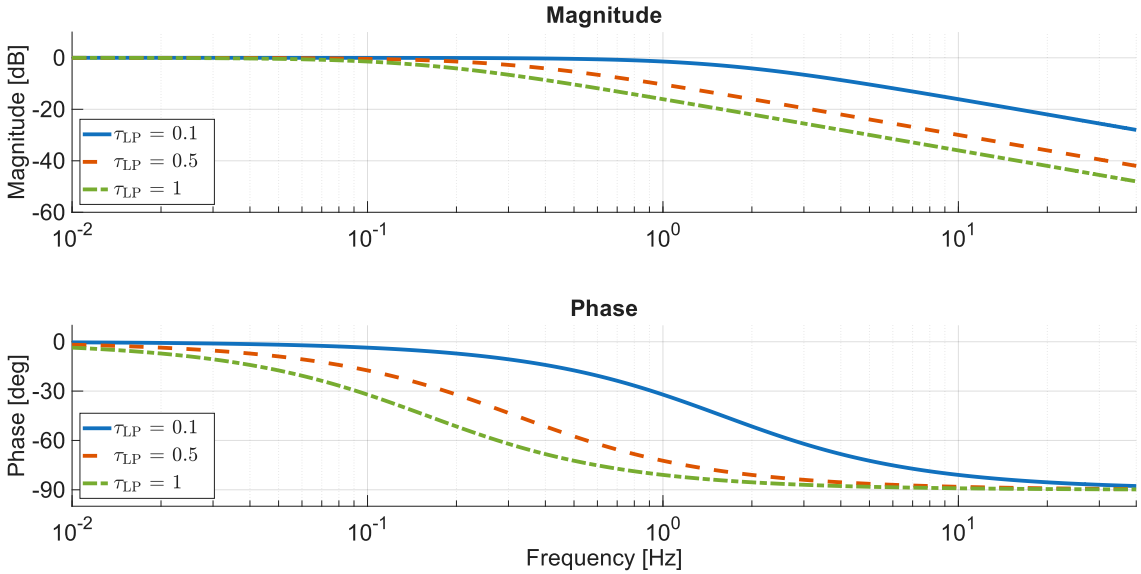

Figure 2.8: Bode plot of a LP filter for various time constants τ_{LP}.

A MAVG filter operates by taking the average of the most recent samples over a window length of N with a sampling time of T_{s}. The size of the sampling window is determined by the desired filtering time constant τ_{MAVG}. This process suppresses high-frequency noise and transients, as these fluctuations only contribute to a small portion of the overall average [28]. The relation between the sampling time, time constant and window length is found as

$$N = \frac{\tau_{\text{MAVG}}}{T_s}. \tag{2.28}$$

The bode plot of the MAVG filter can be seen in Fig. 2.9. It can be noticed that the specific frequency components which are canceled, correspond to multiples of $1/\tau_{\text{MAVG}}$.

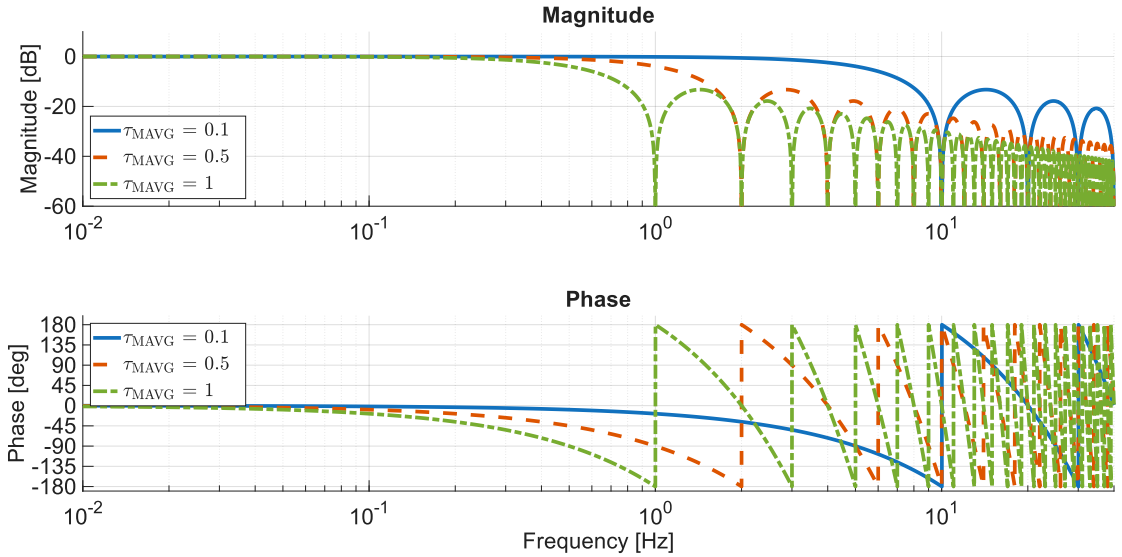

Figure 2.9: Bode plot of a MAVG filter for various time constants τ_{MAVG}.

Another type of filter is the high-pass filter that removes low frequency components and steady state components [29]. The HP filter can be used, e.g. for dynamic FFR, allowing the controller to respond only to fast frequency changes rather than in steady-state. The transfer function of an first order HP filter,

$$H(s) = \frac{s}{s + \omega_c}, \tag{2.29}$$

is very similar to (2.27) but with an s in the numerator instead of the cut-off frequency ω_c. The response of the HP filter for different time constants ($\tau_{\text{HP}} = 1/\omega_c$) is shown in Fig. 2.10.

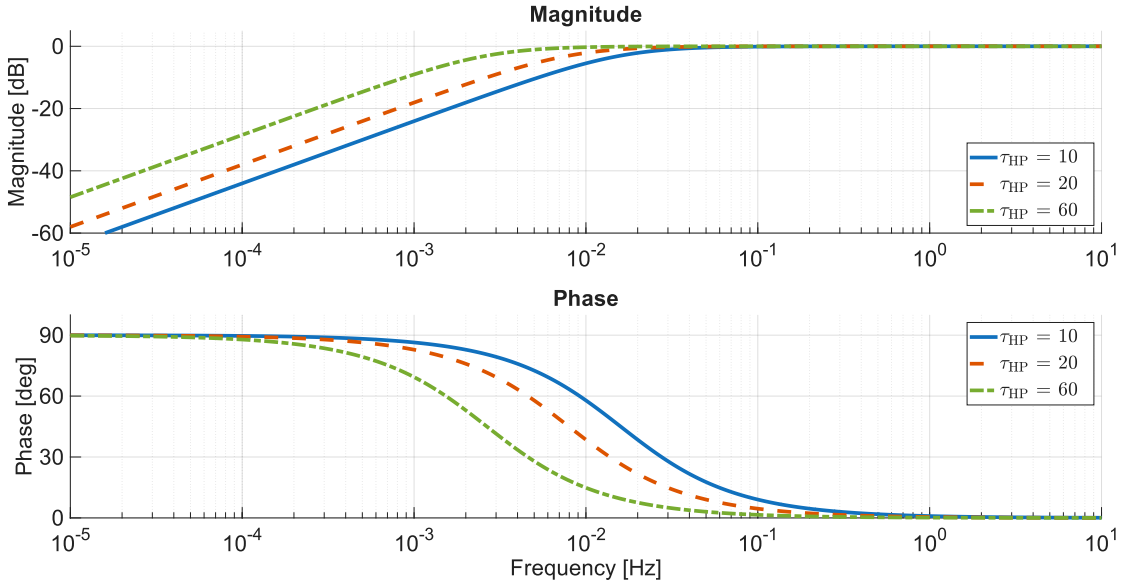

Figure 2.10: Bode plot of a HP filter for various time constants τ_{HP}.

Finally, a lead-lag filter can be used to either attenuate or amplify higher frequencies while allowing lower frequencies to pass [30]. The transfer function of a lead-lag filter is given by

$$H(s) = \frac{1 + sT_1}{1 + sT_2}, \tag{2.30}$$

where T_1 is the zero time constant and T_2 is the pole time constant. The fraction between these time constants determines if and by how much the higher frequencies are amplified or attenuated. For example, if T_1 in (2.30) is set to be smaller than T_2, lead-lag becomes a lag filter, which attenuates higher frequencies. This is seen in the bode plot in Fig. 2.11 where the lead-lag filter attenuates the higher frequencies.

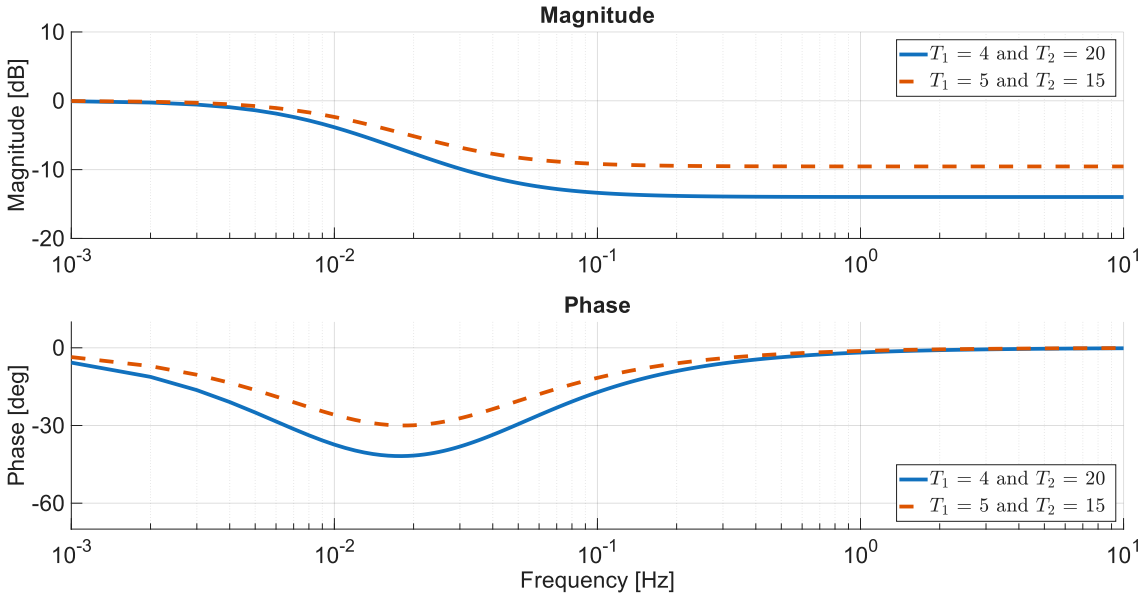

Figure 2.11: Bode plot of a lead-lag filter. The parameters T_1 and T_2 define the attenuation or amplification profile.

From Fig. 2.11 it is shown that the attenuation of higher frequencies is the fraction between T_1 and T_2.

2.9 Technical Requirements for FCR-N

There are multiple requirements for a production unit to be allowed to provide FCR-N, which are defined by ENTSO-E [11]. The requirements include both time domain and frequency domain requirements, which are described in more detail in the following sections. ENTSO-E has not yet published requirements for dynamic FFR and synthetic inertia, as these technologies are not technically mature.

2.9.1 Time Domain Requirements

To determine whether performance in the time domain is valid, steady-state performance, endurance, and dynamic performance are evaluated [11]. To evaluate the performance in the time domain, a step sequence of the frequency is applied as the measured frequency in the FCR controller. The frequency step sequence and an example of the corresponding power response are illustrated in Fig 2.12.

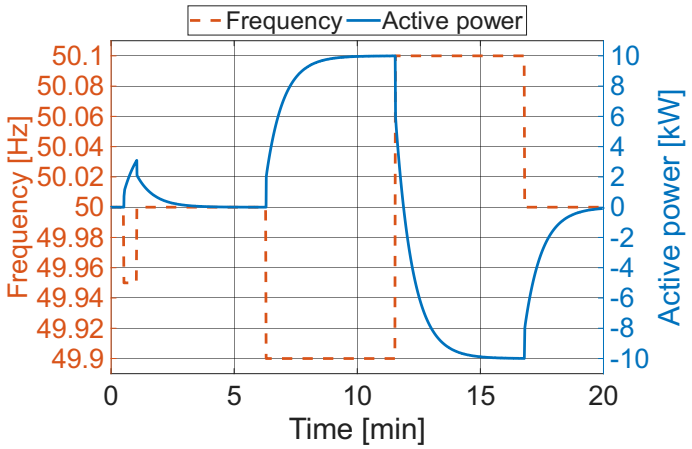

Figure 2.12: Step sequence in frequency with an example of power response, for evaluation of the time domain requirements given by [11].

Firstly, the dynamic performance is evaluated by the rise time of the output power. The requirements in [31] state that during a step of 0.1 Hz, the power should reach 63% of the final value within 60 seconds and 95% within 3 minutes.

Secondly, the endurance test evaluates whether the source is able to support the grid for a certain period of time [11]. Depending on the type has limited energy reservoir or not, the step duration in Fig. 2.12 is longer for non-limited energy reservoirs.

Lastly, steady-state performance evaluates the deviation of the power response from the theoretical response [11]. The requirement for both up- and down regulation states that the maximum under-delivery for either direction is 5% and a maximum of 20% over-delivery.

2.9.2 Frequency Domain Requirements

The frequency domain requirements for FCR-N consist of two criteria, stability and performance. Verifying the requirements is done by injecting a sine wave frequency into the FCR-N controller and evaluating the output power in relation to the frequency input. The time-period of the injected frequency varies between 300 s and 10 s, with a constant amplitude of 0.1 Hz centered around 50 Hz.

The stability and performance in the frequency domain are evaluated by the transfer function of the inverter ($F(s)$) and the grid's ($G(s)$). $G(s)$ is a defined transfer

function specified by ENTSO-E in [11]. $F(s)$ is derived instead from the measured result of the power response by the injected frequency [11].

For the stability requirement, the negative open-loop function is evaluated in a Nyquist diagram. Due to the fact that $F(s)$ is being measured, only certain points of the transfer function are found. Hence, the assumption is made that the transfer function is linear between points. The open-loop function is calculated as

$$G_0(j\omega) = -F(j\omega)G(j\omega), \tag{2.31}$$

where ω is the angular frequency of the injected frequency signal. The technical requirement for FCR-N states that (2.31) should have a margin from the instability point (-1,0) with a radius of 0.43 [11]. However, the stability requirement is also accepted if it has a margin with a radius of 0.4085 from the instability point.

For the performance requirement, the closed-loop transfer function is evaluated instead and in the bode magnitude plot. The closed-loop transfer function is found as

$$G_{\mathrm{c}}(j\omega) = \frac{G(j\omega)}{1 + F(j\omega)G(j\omega)}. \tag{2.32}$$

The criteria, set by ENTSO-E, state that the magnitude of (2.32) with 0.95 scaling shall always be less than the magnitude of the inverse of their disturbance profile $D(s) = |\frac{1}{70j\omega+1}|$, as illustrated in Fig. 4.8 [11].

3

Design and Implementation of Grid Following Inverter for Laboratory Experiments

This chapter begins by defining the per-unit system and its base values. This is followed by a description of the experimental setup, including the inverter, voltage source and network model. Subsequently, the tuning of the various controllers introduced in the Chapter 2 is explained and then the modifications necessary for implementing the control system in the laboratory environment. At the end of Chapter 2 is a summary of all parameters used in the design of the inverter and the parameters for the experiment set-up presented.

3.1 Declaration of the Per-Unit Base

To simplify the control design and thus the calculations, the per-unit (p.u.) system was utilized. The principle of p.u. system is to normalize all quantities with a certain base value. The base units were chosen based on the rated values of the inverter, which had a rated power (S_B) of 10 kVA and a rated phase-phase voltage of 400 V. Furthermore was the power system frequency used as the base frequency. From these quantities, the remaining base values could be calculated. The base current, I_B, and impedance, Z_B, was derived from the apparent power and ohm's law

$$S_\mathrm{B} = \sqrt{3} V_\mathrm{B} I_\mathrm{B} = \frac{V_\mathrm{B}^2}{Z_\mathrm{B}}. \tag{3.1}$$

For the base inductance of the system, the reactance base is equal to the base impedance. Therefore is the base inductance

$$L_\mathrm{B} = \frac{X_\mathrm{B}}{2\pi f_\mathrm{B}}, \tag{3.2}$$

where f_B is the base frequency. Finally, the angular frequency is given by $\omega_\mathrm{B} = 2\pi f_\mathrm{B}$. Together with (3.1) and (3.2), this defines the reaming base values, all of which is presented in Tab. 3.1

Table 3.1: Base values in the power system laboratory.

Variable	Value	Unity
S_{B}	10	kVA
V_{B}	400	V
I_{B}	14.4	A
Z_{B}	16	Ω
f_{B}	50	Hz
ω_{B}	314	rad/s
L_{B}	0.0509	H

3.2 Experiment Setup

In this Section, the setup for the inverter, laboratory and measurements are introduced. The inverter is introduced first and described together with the relevant software. Second, the types of voltage source the inverter operates against are described, followed by the types of network used in between. Last, the adaption of the requirements and studies of the invert is descried.

3.2.1 Inverter Setup

The inverter in the power system laboratory is implemented using a Regatron TC.ACS, which emulates a controllable power supply [32]. The Regatron receives reference voltage control signals calculated by the control system and outputs corresponding AC voltages to the physical network model in the laboratory. It operates in voltage control under amplifier mode, which means that low-voltage analog input signals are amplified.

The control system is implemented using a dSPACE MicroLabBox [33], which requires discrete-time models for real-time operation. Since the controller operates digitally, continuous-time signals must be sampled and processed at discrete time intervals. The MicroLabBox provides Analog to Digital Converters for sampling measurements from the network model and Digital to Analog Converters for sending control signals to the Regatron.

The inverter control system is designed in Simulink using Real-Time Interface blocks to provide inputs and outputs to the MicroLabBox. The Simulink control algorithms are translated into C code, which is executed by the MicroLabBox for real-time control. dSPACE ControlDesk is used as a user interface for parameter tuning and data visualization.

3.2.2 Voltage Source

Two types of voltage sources are used, modeled as V_{g} in Fig. 2.1: a connection to the local power grid and a synchronous generator (SG). The local power grid

is considered a very strong grid, with high short circuit capacity and large system mechanical inertia, which cannot be affected by local changes in power.

In contrast, when the inverter is connected through the network model to the SG, the strength of the grid is limited. The SG has a fixed amount of inertia, with an inertia constant (H_{SG}) of around 5.6 s, which refers to the SG rated power of 75 kVA. The inertia constant for SG referred to the system base is $H = 5.6\frac{75}{10} = 41.7$ s.

The SG is controlled to emulate either a thermal or a hydro power plant. When operating as a thermal power plant, the SG is tightly regulated to provide a fast frequency response, while hydro regulation has a slower response. The regulation difference is presented in the frequency response in Fig. 3.1 when connecting a 4.5 kW load.

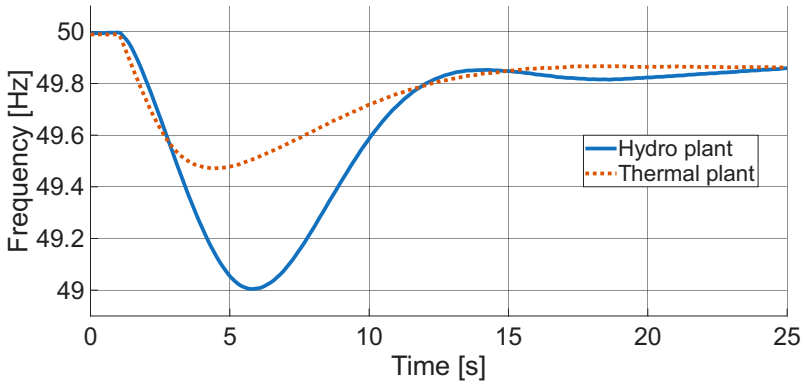

Figure 3.1: Comparison of frequency regulation between an emulated thermal and hydro plant. The dotted line represents the thermal plant, while the solid line shows the response a hydro plant. In both cases, a 4.5 kW load was connected to get a frequency deviation.

As seen in Fig. 3.1, the emulated hydro plant has a lower frequency nadir due to slower regulation and a decrease in power during initial regulation. Furthermore, it is observed that there is an overshoot in the regulation. Lastly, it can be seen that the emulated thermal plant achieves a steady state faster, while the emulated hydro plant has a small damped oscillation.

3.2.3 Network Model

The network model consists of six transmission line sections, or π-sections, that can be utilized. One π-section is characterized by the inductive reactance X_{pi} of 0.953 Ω and the resistance R_{pi} of 0.05 Ω [34]. The capacitance C_{pi} is switched off.

One π-section is used as the inverter's output filter (R_{f} and X_{f}), as shown in Fig. 3.2. The remaining π-sections are used to model the transmission line impedance (L_{g} and R_{g}) between the inverter and the voltage source, as seen in Fig. 3.2. Changing the line impedance is equivalent to changing the line length, where a larger impedance corresponds to a longer transmission line.

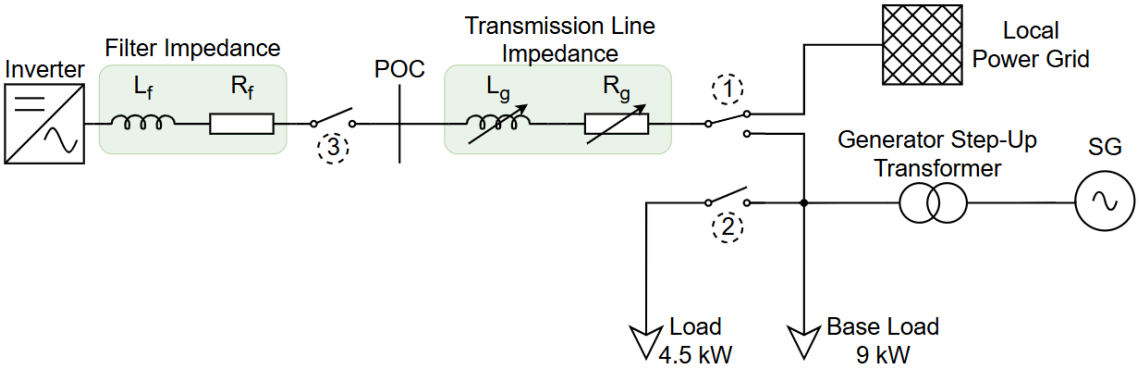

Figure 3.2: The electrical diagram of the experiment setup. With breaker 1 in the upper position, the setup operates in grid-connected mode, while in the lower position it operates in islanded mode. Breaker 2 switches in and out the extra 4.5 kW load. Breaker 3 is used to connect and disconnect the inverter from the experiment setup.

For the case where the inverter is connected to the local power grid, configurations with one, three and five π-sections are investigated. These cases represent strong, intermediate and weak grid conditions that are possible to achieve with the lab setup. Since the local power grid is assumed to be ideal with negligible impedance, the effective grid strength in these scenarios is determined by the number of π-sections. This setup is referred to as grid-connected mode/operation and is achieved when the breaker 1 in Fig. 3.2 is in the upper position. When breaker 1 is in its lower position, the setup operates in islanded mode/operation. In islanded operation, only the SG is used, and a single π-section is used between the POC and SG, since the intention is to study a configuration where the inverter is electrically close to the SG. For the islanded mode, a base load of 9 kW is used and a second load of 4.5 kW can be connected, by closing breaker 2 in Fig. 3.2.

The short circuit impedance for each network combination is calculated and presented in Tab 3.2. The corresponding SCR, calculated according to (2.1), is also shown in Tab 3.2. For islanded operation, a generator step-up transformer with a 1:1 ratio is implemented to introduce the transformer impedance and replicate realistic system behavior. The transformer has a resistance (R_{GSU}) of 0.075 Ω and a reactance (X_{GSU}) of 0.06 Ω. The SG has a resistance (R_{SG}) of 0.081 Ω and a transient reactance (X_{SG}) of 0.437 Ω [34]. Both impedances contribute to the total short-circuit impedance during islanded operation.

Table 3.2: Short circuit impedance and ratios for different scenarios.

Voltage source	π-sections	Short-circuit impedance [Ω]	SCR
Local power grid	1	0.95	17
Local power grid	3	2.86	6
Local power grid	5	4.77	3
SG	1	1.46	11

3.2.4 Operation of Frequency Measurement Devices

In this section, the different methods of measuring the frequency is described. For grid-connected operation, the inverter can operate in two modes, either in measured frequency mode or by simulated frequency mode as indicated in Fig. 3.3. In measured frequency mode, the measured frequency (f_{meas}) is sent to the frequency controller that determines the output power. For simulated frequency mode, a simulated frequency (f_{sim}) is sent to the frequency controller and not the measured frequency. To evaluate the FCR-N technical requirements, the inverter operates in simulated frequency mode. During operation with the SG, only the measured frequency mode is used, and frequency disturbances are performed by connecting or disconnecting the 4.5 kW load.

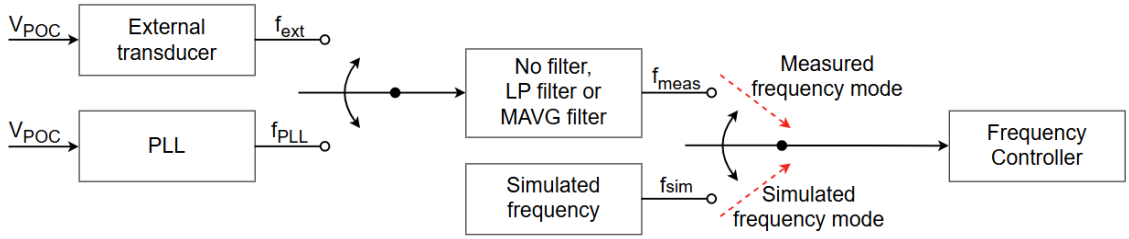

Figure 3.3: Operating in measured frequency mode offers two options of frequency measurement device, a PLL or an external transducer, refereed to as external (see Section 3.5.2). The LP and MAVG frequency filters (previously shown inside the PLL in Fig. 2.3) are moved outside the PLL in this figure to show that both frequency measurement devices can use those filters. Simulated frequency mode utilizes an simulated frequency as the input.

Operating the inverter in measured frequency mode, the disturbance is added by a step in P_{ref}, for the FCR-N and dynamic FFR controller. While evaluating the synthetic inertia, a ramp is added to the measurement signal. When operating in measured frequency mode, the stability of the inverter is evaluated considering the regulating strength, inertia constant and filtering of frequency measurement.

Due to the inverter's fast response time, the FCR-N technical requirements have been performed in a shorter time frame. For the time-domain requirements, the step-sequence is scaled down from minutes to seconds while the frequency-domain requirements has fewer number of cycles per period. Furthermore, three additional periods was added 5, 1 and 0.5 s, to further evaluate the performance then specified in [11]. The endurance test in the FCR-N technical requirements was not performed, as this thesis does not consider limitations in energy storage.

3.3 Controller Tuning

The tuning of the controller is performed such that the outer loops are slower than the inner loops, otherwise oscillations and instability may occur in the inverter. The

bandwidth of the controllers are however limited by the switching frequency of the inverter, to 5 kHz [35].

The control system is organized in a cascaded manner, where the inner control loop is enclosed by slower outer control loops, as illustrated in Fig. 2.7. All controllers are tuned after the filter shown in Fig. 3.2. The filter consists of a resistance, R_f of 50 mΩ and inductance, L_f, of 3 mH. Due to the inverter being heavily internally filtered, the output voltage does not require additional filtering. Therefore, the filtering capacitance C_f is neglected.

3.4 Evaluation of Inverter's Control Design

In this section, the operation of the inverter's current and power controller is presented. Both controllers were evaluated with a strong, intermediate, and weak grid, as defined in Section 3.2.3. Furthermore, both types of power controllers, PC-DIV and PC-PI, were evaluated.

3.4.1 Current Controller

The controllers are tuned sequentially, starting from the innermost loop and progressing outwards. Therefore, the current controller is tuned first, as the innermost loop is the fastest controller after the switching. The bandwidth of the current controller was chosen to be one-tenth of that of the inverter's, $f_\mathrm{CC} = 500$ Hz. For stability and to avoid oscillations between the loops, an industry standard is to keep the outer-loop's bandwidth a tenth of the inner-loop's [36]. To determine the integral and proportional gain of the current controller, (2.24) is utilized by inserting the current controller's bandwidth and the filter parameters R_f and L_f. The proportional gain is found to be $K_\mathrm{P,CC} = 1$ p.u. and the integral gain $K_\mathrm{I,CC} = 31$ p.u./s , following (2.24).

The feedback voltages $V^\mathrm{d}_\mathrm{POC}$ and $V^\mathrm{q}_\mathrm{POC}$, shown in Fig. 2.6 were equipped with an LP filter. Since the voltage is directly coupled with the inverter, any high-frequency oscillations or ripples are propagated to the inverter. Therefore, the objective for the LP filter is to suppress very high-frequency components and ripples in the measured voltage, thus, the cut-off frequency ($f_\mathrm{c,FFV}$) was set to 500 Hz for islanded operation and 100 Hz for grid-connected operation. The cut-off frequency for the grid-connected operation had to be reduced to be stable at idle when operating in weak grids.

For the implementation of the current controller in the laboratory environment, active dampening is used by adding a virtual series resistor

$$R_\mathrm{a,pu} = (\frac{2\pi\alpha_\mathrm{cc}L_\mathrm{f,pu}}{\omega_\mathrm{B}} - R_\mathrm{f,pu}) \cdot 0.05 = 0.03 \text{ p.u.}, \tag{3.3}$$

where $L_\mathrm{f,pu}$ and $R_\mathrm{f,pu}$ are the filter impedance L_f and R_f in per-unit.

Active damping attenuates the oscillation in the inverter's controller that could be caused by the fast current controller [37]. The scaling factor is set to 0.05 to provide a moderate amount of active damping.

To verify the operation of the current controller, a reference step in $I_{\text{ref}}^{\text{d}}$ of 0.1 p.u. is performed in the current controller when operating the inverter in grid-connected mode with a weak, intermediate and strong grid. The reference step and measured Id are presented in Fig. 3.4.

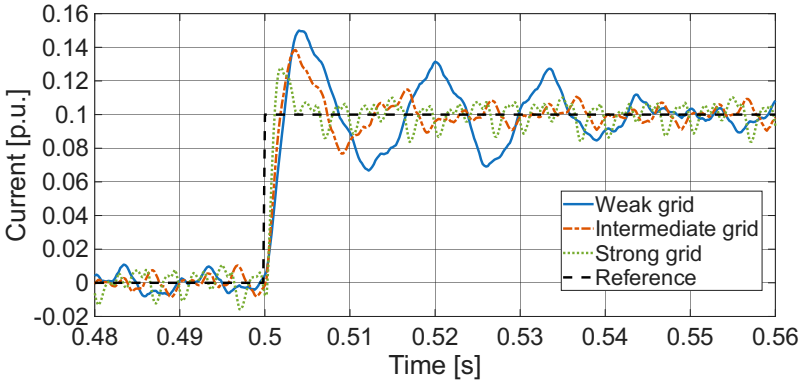

Figure 3.4: Response of inverter's d-component of current output at a reference step of 0.1 p.u. The dashed line presents the step in reference current and the solid, dash-dotted and dotted line shows the corresponding output current for a weak, intermediate and strong grid

From the measured output current, the time constant of the response was found to be around $\tau_{\text{actual,CC}} = 1.6$ ms, which equals a bandwidth ($f_{\text{actual,CC}}$) of 100 Hz, for all three grid strengths. The practical bandwidth is thus a fifth of the theoretical bandwidth, which could be caused by the delay in the feedback voltage filter, in the estimation of phase angle by the PLL and in the Regatron.

3.4.2 Power Controller

With the current controller tuned, the subsequent controller to tune was the power controller. The bandwidth of the power controller is tuned such that the bandwidth is at least ten times lower than the current controller's [36]. Moreover, the two different controllers are tuned differently because of their different designs. The PC-PI is tuned by the proportional and integral gain, while the PC-DIV is tuned through an LP filter.

For the PC-PI controller, the maximum bandwidth was found to be $f_{\text{PC}} = f_{\text{CC}}/10 = 50$ Hz resulting in a time constant of $\tau_{\text{PC}} = 1/(2\pi f_{\text{PC}}) = 3$ ms. With a proportional gain, $K_{\text{P,PC}}$, of 0.25 p.u./p.u. and an integral gain, $K_{\text{I,PC}}$, of 30 rad/s the time constant of the power controller is 30 ms and the bandwidth 5 Hz. The power controller is therefore 10 times slower than the theoretical calculations to allow extra margins for the operation of the power controller. The tuning of the PC-DIV

is achieved by inserting an LP filter at the output and selecting an appropriate cut-off frequency such that the time constant of the PC-DIV is similar to that of the PC-PI. With a cut-off frequency ($f_{\text{c,PC-DIV}}$) of 10 Hz on the LP filter, the resulting time constant of the PC-DIV was 20 ms, corresponding to a bandwidth of 8 Hz.

Furthermore, the PC-PI compares its reference power with the measured power, which is calculated from the measured current and voltage. Consequently, high-frequency components might be introduced into the controller. Therefore, for the implementation of the PC-PI controller in the laboratory environment, the power calculations are equipped with an LP filter. The LP filter has a cut-off frequency ($f_{\text{c,Power calc}}$) of 50 Hz for islanded operation and 20 Hz for grid-connected operation. The cut-off frequency had to be reduced for the grid-connected operation to ensure stable idle operation in weak grids.

Similar to the current controller, the power controller is verified when the inverter operates in grid-connected operation with a weak, intermediate and strong grid. A reference step of 1 p.u. is performed, and the corresponding output power for both the PC-DIV and PC-PI is presented in Fig. 3.5.

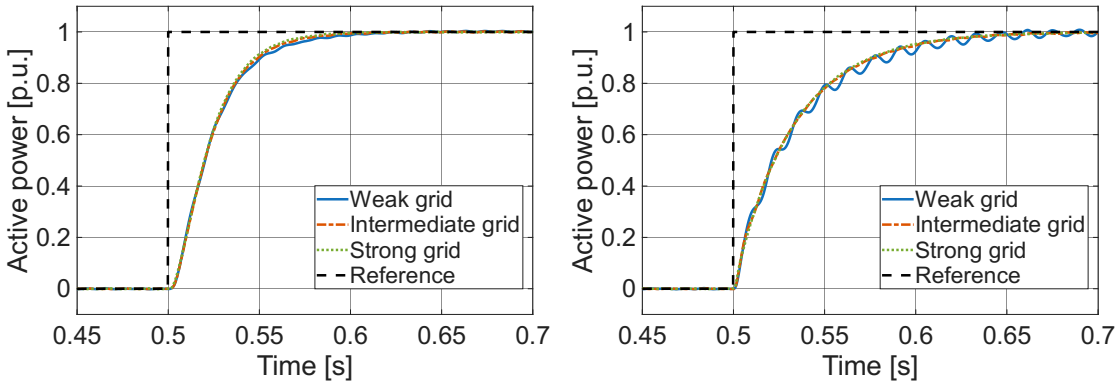

(a) Step response of the PC-DIV **(b)** Step response of the PC-PI

Figure 3.5: The inverter's power output response to a 1 p.u. step in reference power. For both figures, the dashed line represents the reference power, while the dotted, dash-dotted and solid line shows the inverter's measured output power for a strong, intermediate and weak grid.

Evaluating the step response for both controllers, the time constant for all three grid strengths was found to be $\tau_{\text{PC-DIV}} = 25.4$ ms for the PC-DIV and $\tau_{\text{PC-PI}} = 32.6$ ms for the PC-PI. Thus, the bandwidths ($f_{\text{PC-DIV}}$ & $f_{\text{PC-PI}}$) of the controllers are 6 Hz and 5 Hz, respectively. This proves the power controller is operating as intended after the tuning of the PC-PI and PC-DIV.

In Fig 3.5b it is seen that the power output from the PC-PI has small oscillations for weaker grids which the PC-DIV in Fig. 3.5a does not have. This is due to the PC-DIV being equipped with a LP filter at its current reference. With the LP filter, the response from the power controller is smoothed out, thus the inverter increases

it output power smoothly and achieves a stable response. However for the PC-PI the proportional gain generates almost a step in reference, and then the integral part helps smoothen the response. Due to the step from the proportional part the current controller overshoots, initializing the oscillations in voltage. This step from the proprtinal gain is however not visible in Fig. 3.5b since the measured power is filtered through a 50 Hz filter.

3.4.3 FCR-N

From (2.5), the target regulating strength (K_{target}) is found by the inverter's full power range (10 kW) and FCR-N maximum frequency deviation (0.1 Hz) to be 500 p.u./p.u. (which is the same as 1000 %/Hz or 100 kW/Hz). The FCR-N controller is equipped with an LP filter at the output with a cut-off frequency of 10 Hz to attenuate any high frequency-component from the frequency measurement.

Due to the inverter having a rapid response, a lead-lag filter can be enabled in the FCR controller to improve the maximum regulating strength. The lead-lag filter is placed after the FCR's LP filter, as shown in Fig. 2.2. For the lead-lag filter, the zero time constant T_1 in (2.30) was set to 4 s, and the pole time constant T_2 was set to 20 s. This configuration is henceforth referred to as the 4/20 lead-lag filter. Consequently, the magnitude of higher frequencies is attenuated to 0.2 of the filter's input level.

3.4.4 Dynamic FFR

The dynamic FFR controller had a similar controller as the FCR, but with a HP filter in cascade with the LP filter. The effect of the HP filter's time constant τ_{HP}, was evaluated by using the time constants 10, 20 and 60 s as in [20].

3.4.5 Synthetic Inertia

For the synthetic inertia controller the maximum inertia was determined from (2.8) and that the rated power where to be delivered at an RoCoF of 2 Hz/s. According to the Requirements for Generators and the Swedish implementation EIFS 2018:2, generators should be able to ride through a fault of a minimum of 2 Hz/s [38]. To minimize the risk of units disconnecting during faults, maximum power is to be delivered at 2 Hz/s. Applying a RoCoF of 2 Hz/s in (2.8), the target synthetic inertia constant (H_{target}) is 12.5 s referred in S_{B}.

3.4.6 Phase-Locked Loop

The phase-locked loop is the outermost control loop and therefore the slowest. The bandwidth of the PLL was determined to be a tenth of the power controller, thus $f_{\text{PLL}} = 5$ Hz. Assuming a critically damped system ($\zeta = 1$), the coefficients of the PLL, calculated by (2.14), are thus

$$\begin{cases} K_{\mathrm{P,PLL}} = 2 \cdot 2\pi f_{\mathrm{PLL}}\zeta = 2\sqrt{K_{\mathrm{I,PLL}}}\zeta = 63 \text{ s}^{-1} \\ K_{\mathrm{I,PLL}} = (2\pi f_{\mathrm{PLL}})^2 = 987 \text{ s}^{-2} \end{cases} \tag{3.4}$$

3.5 Modification for Implementation

To ensure proper operation of the inverter, additional tuning and functions are added. This includes tuning of saturation blocks and presenting a secondary frequency measuring device. These functionalities help increase the stability and robustness of the inverter.

3.5.1 Saturation Blocks

Signal limits were also applied using saturation blocks. Since the inverter is incapable of operating outside its physical limits, digital limitations are needed within the controller. In the FCR-N controller, the maximum reference power is limited to the rated power of the converter, 1 p.u. The same limitation is set on the reference power from the dynamic FFR and synthetic inertia controllers. Furthermore, in the PC-DIV power controller, another saturation block is used to ensure that the denominator, $|V_{\mathrm{POC}}|$, cannot be zero.

In addition to the power limit blocks in the power controller, there are also limits on the reference current. As stated in [39], power generating units are required to be able to deliver nominal power when the voltage is within 90-105%. Thus, during the voltage drop to 0.9 p.u. the current is increased to deliver 1 p.u. of power. Thus, the current limit ($I_{\mathrm{ref,lim}}$) was calculated to $\frac{P_{\mathrm{nominal}}}{0.9V_{nominal}} = \frac{1}{0.9 \cdot 1} = 1.11$ p.u..

A limitation block is also applied to the output of the current controller to keep the voltage references within a safe operating range. As stated in [39] the maximum voltage the inverter should be able to operate in is 105% at the POC. Accounting for the filter impedance (L_{g} and R_{g}) and the maximal current limit of 1.11 p.u., the d- and q-axis voltage references are limited to $V_{\mathrm{ref,lim}} = 1.05 + 1.1 \cdot |R_{\mathrm{g}} + j\omega_{\mathrm{B}}L_{\mathrm{g}}| \approx 1.2$ p.u..

3.5.2 Secondary Frequency Measurement Device, External Transducer

For frequency regulation, the measured frequency is the most critical signal. In Fig. 2.3, the frequency is obtained by the PLL, optionally filtered, and fed to the frequency controller that regulates the reference power. Since frequency measurement is crucial for the inverter's regulation, a modification is introduced to enable the use of an external frequency measurement device. A switch is added between the PLL and the filtering stage to allow selection between the PLL and the external transducer, as presented in Fig. 3.3. The Tillquist LQT400 is used as the external transducer. It is a configurable multi-converter capable of measuring various electrical quantities [40]. LQT400 is configured here to measure the frequency of the grid

and output an analog signal between 4 and 20 mA, corresponding to the frequency interval of 49.5 and 50.5 Hz. To convert the analog current to a voltage, a 250 Ω resistor is used. With a 250 Ω resistor, the 49.5 to 50.5 Hz interval is equivalent to a voltage interval of 1 to 5 V.

3.6 Summary of Model Parameters

This final section summarizes the design parameters for the inverter and the network parameters, which was presented throughout Chapter 3. Tab. 3.3 presents the baseline parameters that used in both grid-connected and islanded operation.

Table 3.3: Compilation of parameters for the inverter controllers and the network model, that is shared between operating in grid-connected mode and islanded operation.

Parameter	Value
Current controller	
f_{CC}	500 Hz
$K_{\text{P,CC}}$	1 p.u.
$K_{\text{I,CC}}$	31 rad/s
R_{a}	0.03 p.u. (0.48 Ω)
$\tau_{\text{actual,CC}}$	1.6 ms
$f_{\text{actual,CC}}$	100 Hz
$V_{\text{ref,lim}}$	1.2 p.u. (480 V)
Power controller	
$K_{\text{P,PC-PI}}$	0.25 p.u./p.u.
$K_{\text{I,PC-PI}}$	30 rad/s
$\tau_{\text{PC-PI}}$	32.6 ms
$f_{\text{PC-PI}}$	5 Hz
$f_{\text{c,PC-DIV}}$	10 Hz
$\tau_{\text{PC-DIV}}$	25.4 ms
$f_{\text{PC-DIV}}$	6 Hz
$I_{\text{ref,lim}}$	1.11 p.u. (16 A)

Parameter	Value
Frequency controller	
K_{target}	500 p.u./p.u (100 kW/Hz)
H_{target}	12.5 s
PLL	
f_{PLL}	5 Hz
ζ	1
$K_{\text{P,PLL}}$	63 s^{-1}
$K_{\text{I,PLL}}$	987 s^{-2}
Network model parameters	
X_{pi}	0.060 p.u. (0.953 Ω)
R_{pi}	0.0031 p.u. (0.05 Ω)
X_{f}	0.060 p.u. (0.953 Ω)
R_{f}	0.0031 p.u. (0.05 Ω)
X_{GSU}	0.0038 p.u. (0.06 Ω)
R_{GSU}	0.0047 p.u. (0.075 Ω)
X_{SG}	0.18 p.u. (2.93 Ω)
R_{SG}	0.051 p.u. (0.081 Ω)
H_{SG}	5.6 s

While Tab. 3.3 covers the shared parameters and the corresponding response time of the controllers, some parameters change depending on the mode. Tab. 3.4 shows these changes, comparing the specific settings used for grid-connected and islanded mode.

Table 3.4: Compilation of parameters for the inverter controllers and the network model, that is specific for each operating condition.

(a) Grid-connected operation

Parameter	Value
Current controller	
$f_{\mathrm{c,FFV}}$	100 Hz
Power controller	
$f_{\mathrm{c,Power\ calc}}$	20 Hz
Network model parameters	
SCR	17, 6 or 3

(b) Islanded operation

Parameter	Value
Current controller	
$f_{\mathrm{c,FFV}}$	500 Hz
Power controller	
$f_{\mathrm{c,Power\ calc}}$	50 Hz
Network model parameters	
SCR	11

Tab. 3.3 and 3.4 shows that the majority of the parameters are shared between the operation modes. However, the SCR is different since, for islanded operation, the battery should be electrically close to the SG and for grid-connected operation, the network between the inverter and the grid is investigated. Additionally, $f_{\mathrm{c,FFV}}$ and $f_{\mathrm{c,Power\ calc}}$ were different because the inverter became unstable for weak grid operation if the islanded mode parameters were applied.

4

Analysis of Stability Limits and Performance for Inverter Providing FCR-N, Dynamic FFR and Synthetic Inertia

This chapter presents the results of stability limits and performance for FCR-N, dynamic FFR and synthetic inertia. Since not all frequency controllers are evaluated for stability limits and performance, nor are all evaluated in both grid-connected and islanded operation, Tab. 4.1 presents a summary of the analyzes performed and their corresponding section.

Table 4.1: The frequency ancillary services tested against different grid combination, that the result presents.

	Grid-connected operation		Islanded operation	
	Stability limits	Performance	Stability limits	Performance
FCR-N	4.1 & 4.2	4.2	4.3	4.3 & 4.4
Dynamic FFR				4.5 & 4.7
Synthetic inertia	4.6			4.7

When operating in either grid-connected mode or islanded mode, the shared settings used are presented in Tab. 3.3, which is complimented by either Tab. 3.4a when operating in grid-connected operation or Tab. 3.4b when operating in islanded operation. The stability limits and performance of the different frequency ancillary services are evaluated by different types of frequency measuring devices, frequency filtering and type of voltage source used. Therefore, has all the different parameters been compiled in a sensitivity analysis list:

- **Frequency measurement device:** PLL, external transducer
- **Frequency filtering:** unfiltered ($\tau_{\mathrm{LP}} = \tau_{\mathrm{MAVG}} = 0$ s), LP filter, MAVG filter
- **Frequency filter time constant:** 0 s to 1 s
- **Lead-lag filter implementation**
- **Voltage source:**
  - Local power grid, grid-connected operation (SCR 17, 6, 3)
  - SG, islanded operation (SCR 11)
- **Frequency controller:** FCR-N, dynamic FFR, synthetic inertia
- **Control parameters:** regulating strength, synthetic inertia constant
- **Power Controllers:** PC-DIV, PC-PI

In the sensitivity analysis list, the control parameters is used to evaluate the stability limits for the appropriate frequency controller. For the stability limit analysis of the regulating strength, the maximum limit was set to 1000 p.u./p.u. (200 kW/Hz). While for the synthetic inertia constant the limit was set to 200 s. An analysis of the different power controllers where performed in section 4.1-4.3, which showed the operation difference being small and thus only the PC-DIV was used in the subsequent sections.

4.1 Stability for FCR-N in Grid-Connected Operation

The performance of the inverter in grid-connected operation for FCR-N is evaluated by operating the inverter in measured frequency mode and applying a step in the frequency reference. The resulting power response from such a step has been classified into two categories, stable and unstable. The regulating strength was varied for each combination of filter type, filter time constant and frequency measuring device in order to determine the transition between stable and unstable operation. The maximum regulating strength was defined as the regulating strength corresponding to a response that was on the verge of instability, in other words, the critical stable response. The responses shown in Fig. 4.1 are representative examples used to illustrate critical and unstable response characteristics and do not correspond to the same frequency step, filter type, filter time constant, frequency measurement device, or regulating strength.

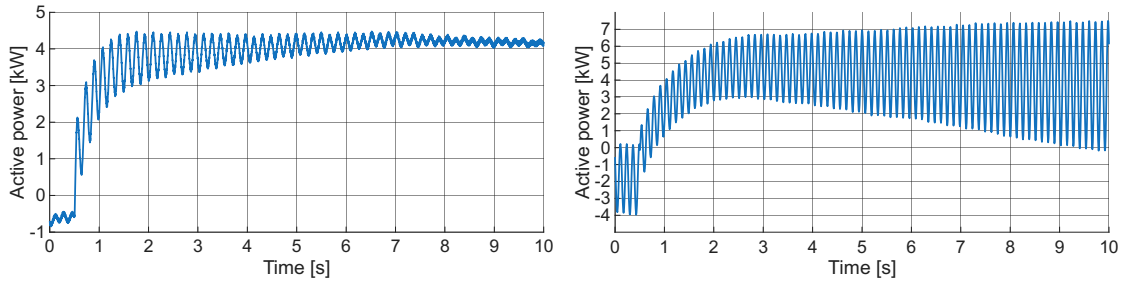

(a) Critically stable power response **(b)** Unstable power response

Figure 4.1: Representative power responses of the inverter during FCR-N operation in measured frequency mode after a step change in the reference frequency. The responses are classified as stable and unstable. The examples shown do not use the same frequency step, regulating strength, filter type, filter time constant, or frequency-measuring device, but are included to illustrate the classification method.

The critically stable response exhibits oscillations that are attenuated over time and eventually reach a steady state, meaning that the inverter control is still capable of damping the oscillations. The unstable response either has growing oscillations or never reaches a steady-state value. Therefore, it is desired to have large margins between the instability limit and the operation point, to have a fast and damped response from the inverter and to not risk instability if the grid changes. The maximum regulating strength is evaluated for strong, intermediate and weak grid conditions as defined in Section 3.2.3.

In Fig. 4.2, the difference between operating the inverter with the PC-DIV and PC-PI in a weak grid (SCR 3), equivalent to operating with a long transmission line, is presented. The stability is assessed for both PC-DIV and PC-PI when measuring the frequency directly from the PLL or from the external transducer, and for the unfiltered, LP or MAVG filtered measured frequency. For unfiltered frequency measurement, the filter time constant is set to 0 s.

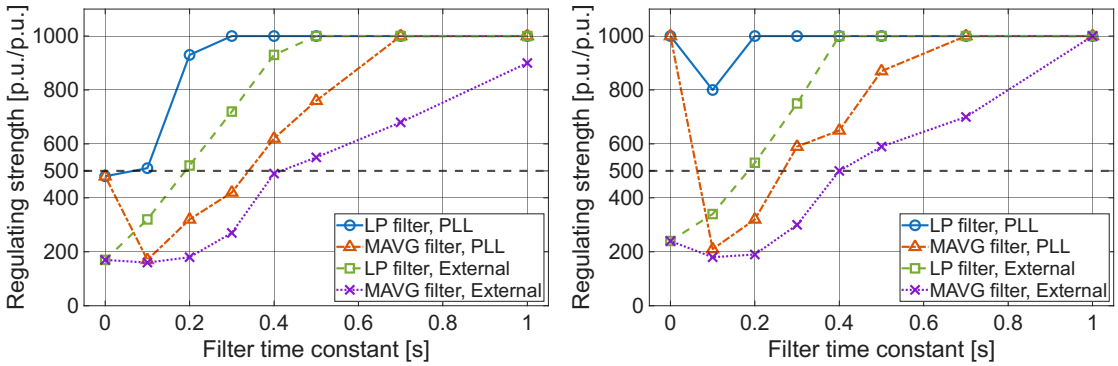

(a) PC-DIV configuration **(b)** PC-PI configuration

Figure 4.2: The maximum regulating strength as a function of the frequency filtering time constant, in a weak grid with the two types of power controllers. Different combinations with PLL or external transducer with unfiltered ($\tau_{\mathrm{LP,MAVG}} = 0$ s), LP or MAVG filtered frequency. The horizontal dashed line indicate the targeted regulating strength of 500 p.u./p.u. (100 kW/Hz).

As described in Section 3.4.3, the maximum evaluated regulating strength is limited to 1000 p.u./p.u. (200 kW/Hz), resulting in a factor of two margin from the desired regulating strength of 500 p.u./p.u. (100 kW/Hz) derived in Section 3.4.3. From Fig. 4.2, the instability of the inverter occurs at low filtering time constants, this is due to rapid changes in the phase angle. At low filtering time constants, the inverter reacts quickly to smaller frequency variations, leading to a rapid change in power output. With a fast change in power, the phase angle in the POC increases, leading to a momentarily local frequency deviation, $f = \frac{1}{2\pi}\frac{d\theta(t)}{dt}$. Consequently, since the inverter operates with a lower filtering time constant, this local frequency deviation is measured and fed back into the control-loop, which creates a positive feedback with high enough regulating strength or low time constant.

Furthermore, from Fig. 4.2 it is seen that the MAVG filter achieves lower stability margins than the LP filter. This is due to the phase-shift of the MAVG filter not limited to -90 degrees as for the LP filter but continuous decreases after -90 degrees, as seen in Fig. 2.8 and 2.9. The phase-shift from the MAVG causes the inverter to compensate for the local frequency deviation out of phase earlier than compared to the LP filter, thus the MAVG is more prone to cause instability. From Fig. 4.2, it is also found that the maximum regulating strength increases between applying lower filtering time constants and unfiltered ($\tau_{\mathrm{MAVG}} = 0$ s). The improvement of stability is caused by the elimination of phase-shift with unfiltered measurements.

In Fig. 4.2 it is seen that the external transducer achieves a lower maximum regulating strength than the PLL, which is due to the external transducer (Tillquist, LQT400) induces phase-shifts and delays into the control-loop. The phase-shifts and delays are caused by the method of measuring the frequency and any internal filtering. The precise phase-shifts and delays the external transducer introduces are not presented, since neither does the manufacturer specify which measuring method is

implemented, nor was the phase-shift and delay of the specific transducer measured.

Comparing the two power controllers (PC-DIV and PC-PI), the difference between their maximum regulating strengths is very small. The only major difference in maximum regulating strength is for the PLL cases with unfiltered and LP filter with a 0.1 s time constant, where the PC-DIV underperforms the PC-PI. This is unexpected since a LP filter should have a gradual decrease in achieved regulating strength. Seen from (2.27) and Fig. 2.8, the characteristics of an LP filter have a limited phase-shift and an inverse relation with the time constant. Thus, if the stability margins was reduced for the 0.1 s time constant it should have been reduced for the unfiltered as well, which is seen in the other result when using the LP filter.

In Fig. 4.3, the maximum regulating strength for both the PC-DIV and PC-PI are presented. The overall difference in maximum regulating strength is negligible between the two power controllers.

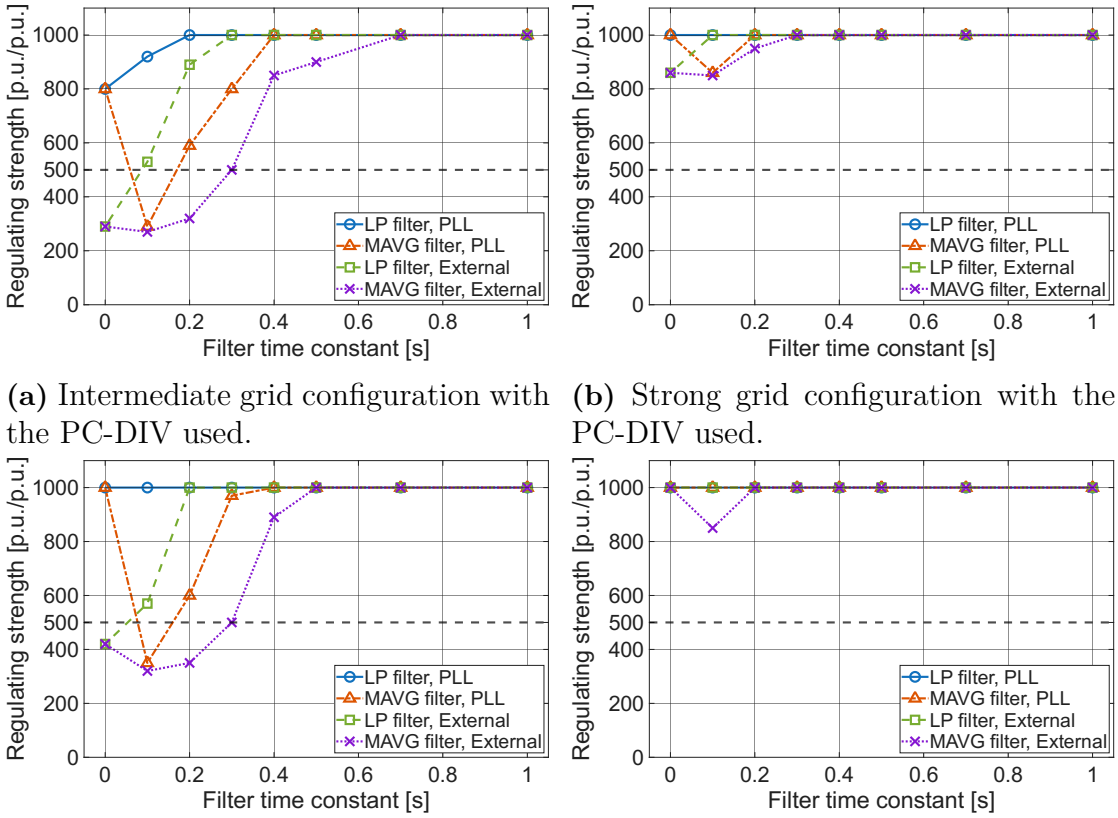

(a) Intermediate grid configuration with the PC-DIV used.

(b) Strong grid configuration with the PC-DIV used.

(c) Intermediate grid configuration with the PC-PI used.

(d) Strong grid configuration with the PC-PI used.

Figure 4.3: The maximum regulating strength as a function of the frequency filtering time constant, for the same combinations as in Fig 4.2a, but for an intermediate and strong grid configuration. Both PC-DIV and PC-PI is evaluated together with the PLL or the external transducer with unfiltered, LP or MAVG filtered frequency. The horizontal dashed line indicate the targeted regulating strength of 500 p.u./p.u. (100 kW/Hz).

It can be seen that a stronger grid improves the stability of the inverter for all filtering setups. Similarly to the results presented in Fig. 4.2a, configurations using the PLL for frequency measurements achieves a higher maximum regulating strength than the configurations using an external transducer. Furthermore the LP filter achieves higher regulating strengths than the MAVG filter independent of the frequency measurement method.

To improve the stability of the inverter, the 4/20 lead-lag filter described in Section 3.4.3, is enabled. Thus, the high-frequency components are attenuated and a smoother and stable response is achieved. The effect of the 4/20 lead-lag filter is presented in Fig. 4.4 when applied to the unstable case shown in Fig. 4.1b.

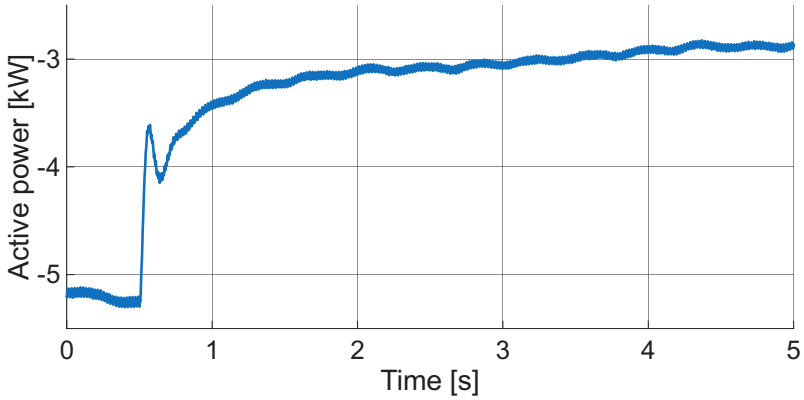

Figure 4.4: The effect of the 4/20 lead-lag filter has on the active power output on the unstable response presented in Fig. 4.1b.

Fig. 4.4 shows that an otherwise unstable case can become stable when implementing the 4/20 lead-lag filter. This stability is achieved because the higher frequency components shown in Fig. 4.1b are attenuated, leading to reduced oscillations. By enabling the 4/20 lead-lag filter, the regulating strength reached 1000 p.u./p.u. (200 kW/Hz) for almost all scenarios presented in Fig. 4.2 and 4.3 with both power controllers. The only exceptions occurred under weak grid conditions for the following cases:

- Using the PC-DIV power controller without frequency filtering.
- Setups using the MAVG filter with a time constant of 0.1 s for both power controllers.
- The combination of the PC-DIV controller, the external transducer, and MAVG filtering with a 0.2 s time constant.

As shown in Fig. 4.2, these specific cases initially had a regulating strength below (or near) $\frac{4}{20} \cdot 1000 = 200$ p.u./p.u. without the 4/20 lead-lag filter. This suggests that the chosen time constants of the 4/20 lead-lag filter would need further tuning to achieve a regulating strength of 1000 p.u./p.u. (200 kW/Hz).

4.2 Technical Requirements for FCR-N

This section presents the result of the evaluation based on the technical requirements for FCR-N following ENTSO-E's guidelines, detailed in Section 2.9. The first part presents the result for the time domain requirements and the second part for the frequency domain requirements.

4.2.1 Time Domain Requirements

A step-sequence is conducted to evaluate the steady-state and dynamic performance of the inverter. Without the lead-lag filter enabled, the sequence was shorten to take 20 s. However, with the 4/20 lead-lag filter, the test duration is changed to 600 s due to the lead-lag filter's slower response. The result with PC-DIV, with or without the 4/20 lead-lag filter, is presented in Fig. 4.5 using a weak grid (SCR of 3).

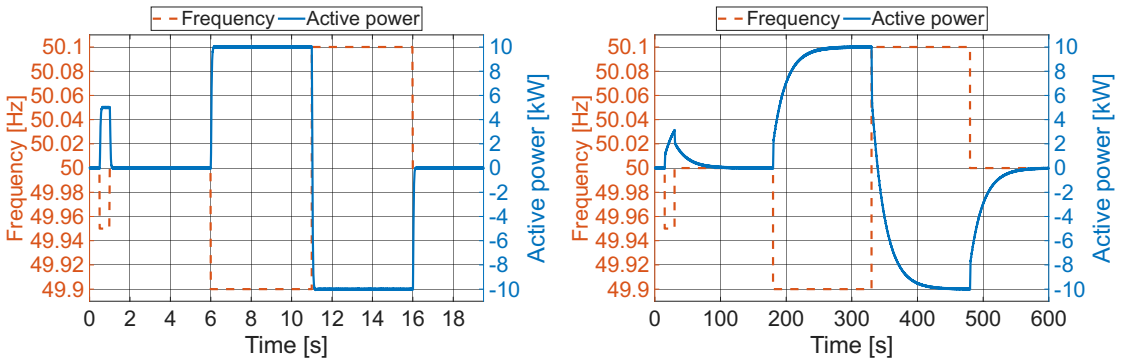

(a) Without 4/20 the lead-lag filter **(b)** With 4/20 the lead-lag filter

Figure 4.5: The simulated frequency (dashed, orange) following the adjusted FCR-N step response sequence, presented together with the inverter's output power (solid, blue). The presented result shows the inverter operating in a weak grid with the PC-DIV.

The difference in the result between different grid strengths and power controllers was found to have negligible effect. The dynamic performance criteria to achieve 63% before 60 s where fulfilled since the longest response took 50 ms. The criteria to reach 95% in less than 3 minutes, were also satisfied, as seen in Fig. 4.5a. For up- and down-regulation, the criteria to not under-deliver less than 5%, or over-deliver more than 20%, where achieved since the maximum up-regulation deviation was found to be 0.01% and 0.02% for down-regulation.

When adding the 4/20 lead-lag filter, the response was much slower, as seen in Fig. 4.5b. For all combinations of grid strengths and power controllers, the maximum time constant was 20 s, and the up- and down-regulation deviations were 0.07% and 0.2%, respectively. This shows that for the dynamic performance requirement, the time to reach 63% of its final value is well below 60 s. Furthermore, the criteria to reach 95% of the steady state in three minutes were met, as seen in Fig. 4.5b.

Additionally, the steady-state requirement was satisfied, not to under-deliver less than 5%, or over-deliver more than 20%.

During the time domain requirements, the frequency filters were bypassed. Therefore, the impact of an LP or MAVG filter was not presented. However, this would not affect the fulfillment of the time domain requirements. This is because with the 4/20 lead-lag filter, the results had large margins from the requirements limits, as shown in Fig. 4.5. Consequently, the influence of any frequency filter would not change the result to exceed the requirements. However, for the frequency domain requirements, the effects of the different filters were evaluated by adding their transfer function to the measured transfer function of the inverter.

4.2.2 Frequency Domain Requirements

For the frequency domain stability requirement, the result with PC-DIV in a weak grid, with the 4/20 lead-lag filter disabled and a frequency filtering time constant of 1 s, is presented in Fig. 4.6. The impact of using PC-PI instead of PC-DIV was found to have a negligible impact. For all cases, a regulating strength of 500 p.u./p.u. (100 kW/Hz) was used.

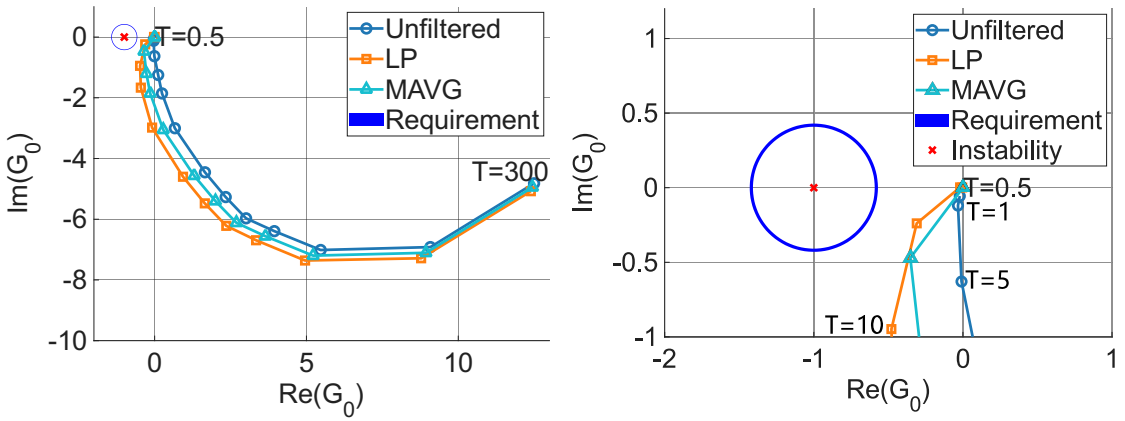

(a) Nyquist diagram showcasing all time periods

(b) Nyquist diagram with focus on the instability point, with the time periods 0.5, 1 and 5 s visible for all three filters and 10 s for LP filter is visible.

Figure 4.6: Nyquist diagram of the frequency domain stability requirement in a weak grid, using PC-DIV with a frequency filtering constant of 1 s. The instability point (-1, 0) is presented in both figures, and in detailed view in (b). Results for the filter methods unfiltered, LP or MAVG filter is marked with circles, squares and triangles, respectively.

In Fig. 4.6b, it is clearly shown that the inverter meets the criteria. With the 4/20 lead-lag filter enabled, the short time periods are shifted closer to origin, as can be seen in Fig. 4.7. From ENTSO-E criteria, the smallest time period to evaluate where 10 s, and comparing Fig. 4.6b and 4.7b higher time periods are now visible, meaning less margin until instability following ENTSO-E's requirement. However the added time periods is closer the origin, and thus farther from the instability limits, which increases the stability margins for small time periods.

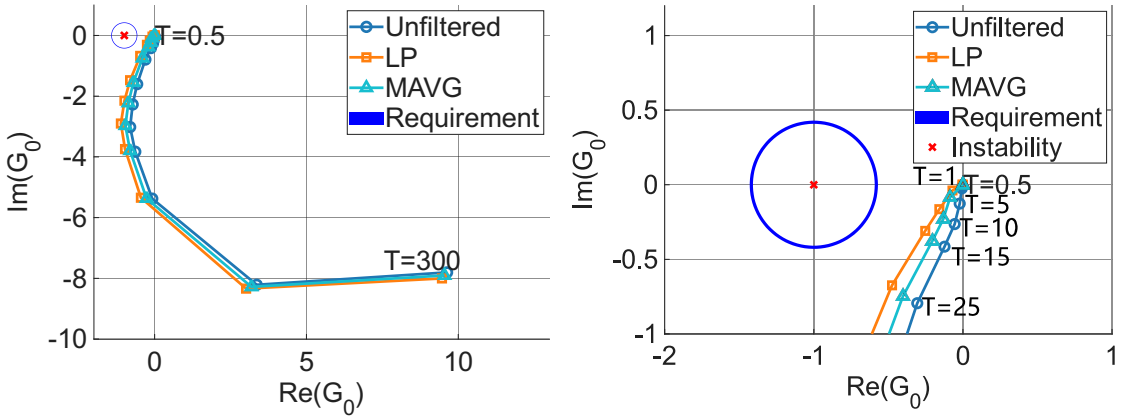

(a) Nyquist diagram showcasing all time periods

(b) Nyquist diagram with focus on the instability point, with the time periods 0.5, 1, 5, 10, 15 and 25 s visible.

Figure 4.7: Nyquist diagram of the frequency domain stability requirement in a weak grid, using PC-DIV with a frequency filtering time constant of 1 s and the 4/20 lead-lag filter enabled. The instability point (-1, 0) is presented in both figures, and in detailed view in (b). Results for the filter methods unfilter, LP or MAVG filter is marked with circles, squares and triangles, respectively.

For Fig. 4.7b the time periods up to 25 s can now be seen, in contrast to Fig. 4.6b. By decreasing the frequency filter time constant from 1 to 0.1 s, the data points becomes closer to unfiltered result. Therefore, since the unfiltered results have larger stability margins, lowering the filtering time constant increases the stability margins.

Lastly, the frequency domain performance criteria with the 4/20 lead-lag filter both enabled and disabled are presented in Fig. 4.8. The presented result uses the same inverter setups as Fig. 4.6 and 4.7.

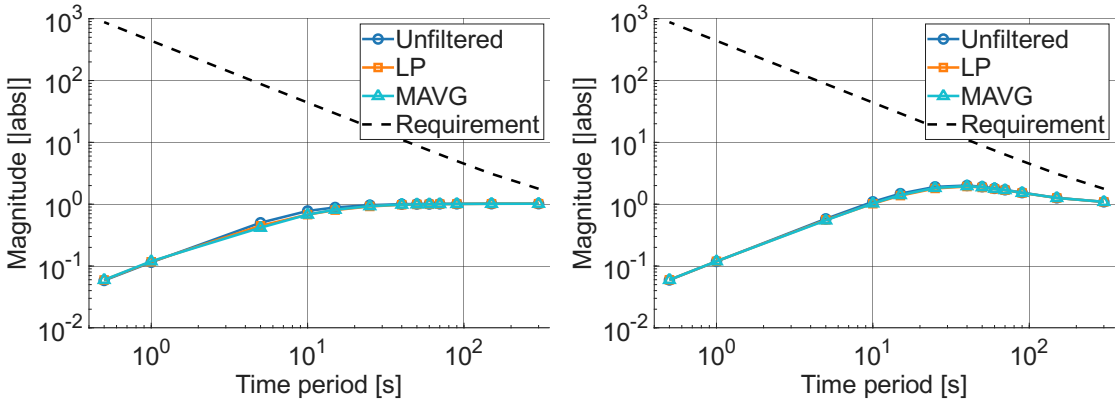

(a) Without a lead-lag filter **(b)** With the 4/20 lead-lag filter

Figure 4.8: The Bode magnitude plot of the frequency domain performance requirement in a weak grid, using PC-DIV with a frequency filtering constant of 1 s, with and without the 4/20 lead-lag filter. The dashed line presents the disturbance profile $D(s)$ and the circle, square and triangle points represents the use of different frequency filters.

From Fig. 4.8a, it can be seen that the inverter satisfies the performance criteria. When applying the 4/20 lead-lag filter the performance requirement is fulfilled. However, the magnitude of the data points from the time period's in the interval 10 to 150 s has increased, as seen in Fig. 4.8b. The magnitude increase in performance is due to the induced phase-shift from the 4/20 lead-lag filter. As seen from the bode diagram of the 4/20 lead-lag filter in Fig. 2.11, the phase-shift is within the time periods 10 to 150 s. Therefore, the performance during the 10 to 150 s interval has changed while using the lead-lag filter.

Furthermore, the impact of performance criteria with a filter time constant of 0.1 s instead of 1 s was not noticeable. In Fig. 4.8 the LP and MAVG filter had a result similar to unfiltered. Therefore, when decreasing the filtering time constant the filters become more unfiltered, hence the difference between the time constant 0.1 s and 1 s was minimal.

In summary, the stability and performance limitation of the inverter is not determined by the type of frequency filter method or the filter time constant. Instead, stability limitations and performance are defined by tuning between the regulating strength and the filter time constant, as seen in Fig. 4.2 and 4.3. Furthermore, since the requirements are fulfilled with margins when using the lead-lag filter, as seen in Fig. 4.5b, 4.7 and 4.8b, and the regulating strength margins reaches 1000 p.u./p.u. (200 kW/Hz) for the majority of all cases, it is recommended to implement a lead-lag filter.

4.3 Stability for FCR-N in Islanded Operation

To evaluate the maximum regulating strength in islanded operation, the inverter operates in measured frequency mode, i.e. the frequency is measured with the PLL or the external transducer. The SG's frequency regulation is disabled by using a deadband of ±3 Hz of nominal frequency. The SG still provides inertia to the system, but it is the inverter that will provide frequency reserve P_{m} in the Swing equation (2.6), when P_{e} changes. Thus, when a load of 4.5 kW is applied, all frequency regulation is done through the inverter. The measured frequency during the 4.5 kW step is presented in Fig. 4.9, both with and without the 4/20 lead-lag filter enabled.

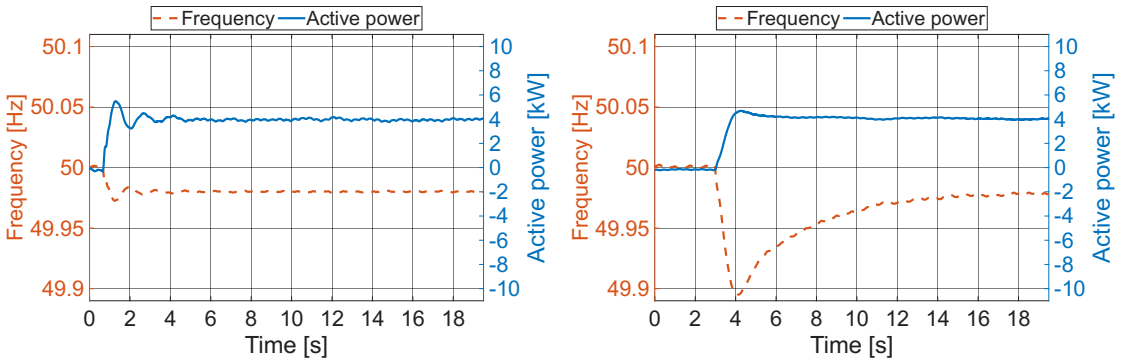

(a) Without the 4/20 lead-lag filter **(b)** With the 4/20 lead-lag filter

Figure 4.9: The frequency and power response of the inverter when it is the only frequency regulation unit in island operation during a load activation of 4.5 kW, with a regulating strength of a 1000 p.u./p.u. (200 kW/Hz). The inverter operates with the PC-DIV and measures the frequency through the PLL and filters the frequency through an LP filter with a time constant of 0.1 s.

Firstly, even though the inverter is a GFL, it can regulate the frequency on its own after the grid has been initialized. As illustrated in Fig. 4.9a, the inverter regulates the frequency to a steady state, despite minor overshoots and oscillations in power response. By adding the 4/20 lead-lag filter in Fig. 4.9b, the frequency nadir is lower, but there are no power oscillations and a smaller overshoot.

The maximum regulating strength was evaluated against the frequency filter time constant in islanded mode. Fig. 4.10 presents the result of maximum regulating strength for combinations of power controllers, frequency measurement, frequency filters and no lead-lag filter. The minimum filtering time constant investigated was reduced from 0.1 s to 0.05 s, to achieve greater resolution at the lower range.

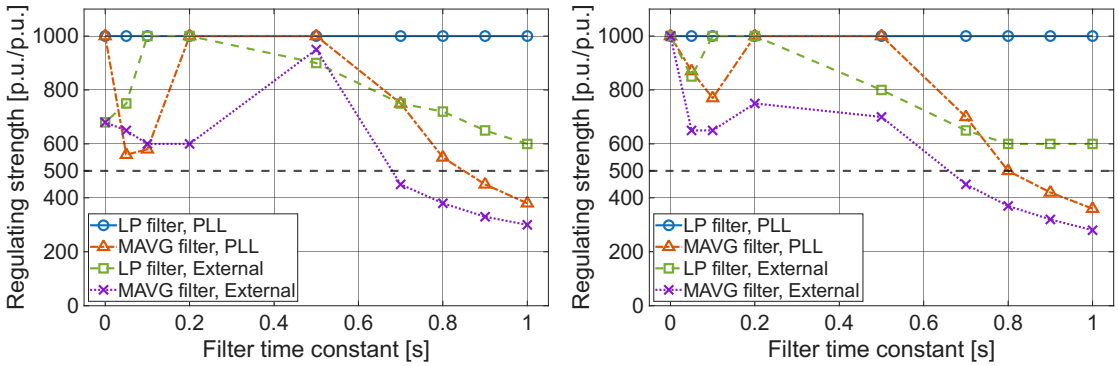

(a) PC-DIV configuration **(b)** PC-PI configuration

Figure 4.10: Maximum regulating strength in islanded operation as a function of the frequency filtering time constant, for different power controllers. The horizontal dashed line indicate the targeted regulating strength of 500 p.u./p.u. (100 kW/Hz). Note that both unfiltered ($\tau_{\mathrm{LP}} = \tau_{\mathrm{MAVG}} = 0$ s) cases in (b) reached a regulating strength of 1000 p.u./p.u. (200 kW/Hz)

The inverter stability is more sensitive to the time constant in islanded operation than in grid-connected mode, since it is more unstable at both high and low filtering time constants. This is clearly shown in Fig. 4.10, except for the LP filter with the PLL since it reaches 1000 p.u./p.u. (200 kW/Hz) for all time constants. The result of Fig. 4.10 behaves similarly to that of Fig. 4.2, that the effect of the power controller is small and the LP filter performs better than the MAVG filter, since the phase-shift of the LP filter is limited between 0 and -90 degree. With the 4/20 lead-lag filter, the regulating strength reached a value of 1000 p.u./p.u. (200 kW/Hz) for all combinations presented in Fig. 4.10.

As could be seen in Fig. 4.10, the system could be unstable for both high and low time constants without the lead-lag filter. Fig 4.11 illustrates two examples of system instability, one with a low filter time constant and one with a high filter time constant. Both examples were obtained using the PC-PI, measuring the frequency through the PLL and using a MAVG filter.

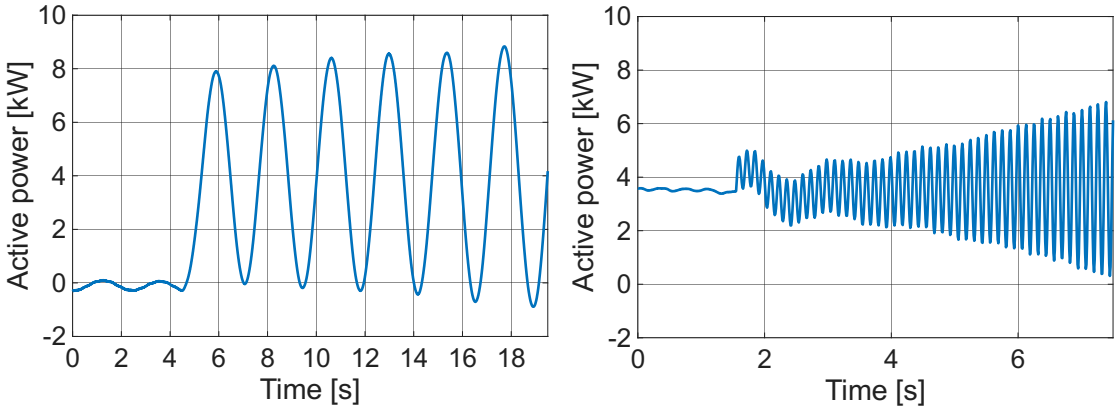

(a) Power response following the connection of a 4.5 kW load, with a filter time constant of 1 s.

(b) Power response with a filter time constant of 0.05 s, showing instability initiated by a change in regulating strength at $t = 1.5$ s up to 900 p.u./p.u.

Figure 4.11: Power response characteristics of the inverter during FCR-N operation, illustrating two unstable cases. The examples are acquired using the PC-PI, measuring the frequency through the PLL and using a MAVG filter.

The causes behind decreased stability for low filtering time constants and increased stability of unfiltered follows a similar reasoning as detailed in Section 4.1. With low filtering time constant the inverter rapidly injects power, that changes the phase-angle leading to local frequency change which is positively feedback into the loop, creating instability. Since the instability occurs due to the inverter compensating for its own phase-shift, the oscillation is of a high frequency as seen Fig. 4.11b whose frequency is around 8 Hz. For high filtering time constants however the instability was caused by oscillation between the inverter and generator, this lead to an slower oscillation, as seen in Fig. 4.11a whose oscillation frequency was around 0.4 Hz. Increasing the filter constant slows down the inverter's response and degrades the phase margin within the frequency control loop. This reduction in phase margin causes the compensation to become out of phase with the power delivery. The interaction worsens as the SG attempts to track the frequency, creating oscillations between the SG and base load that the inverter repeatedly tries to counteract.

4.4 Frequency Regulation by both Inverter and Synchronous Generator

In Section 4.3 the SG operated with a deadband, and thus the inverter performed all the frequency regulation. However, this section presents the result when both provide frequency regulation. The inverter's frequency regulation operates with the FCR-N controller, with the regulating strength determined by the relation to the SG's regulating strength. The relation between the inverter's and SG's regulating strength determines each unit's contribution to frequency regulation. With the SG's regulating strength set to 150 p.u./p.u. (30 kW/Hz), the inverter's regulating

strength was determined to be equal (1:1), twice (1:2) or a third (3:1) of the SG's, which is presented in Tab. 4.2.

Table 4.2: Regulating strengths for three SG to inverter ratios.

SG to Inverter ratio	Inverters regulating strength [p.u./p.u.]	[kW/Hz]	SG regulating strength [p.u./p.u.]	[kW/Hz]
1:1	150	30		
1:2	300	60	150	30
3:1	50	10		

The result for both units contributing to the frequency regulation is presented in Fig. 4.12, when using the 9 kW base load and adding a 4.5 kW load. The inverter operates with the PC-DIV, filters the frequency from the PLL with an LP filter with a time constant of 0.1 s, without any lead-lag filter and operates in islanded mode. As described in Section 3.4.3, for the FCR-N controller to operate within ±0.1 Hz the regulating strength must be 500 p.u./p.u. (100 kW/Hz). With a lower regulating strength, the frequency operation band increases, while it decreases with higher regulating strength, as seen by (2.5). Therefore, with the regulating strengths detailed in Tab. 4.2, the inverter is able to operate outside the ±0.1 Hz interval, as seen in Fig. 4.12.

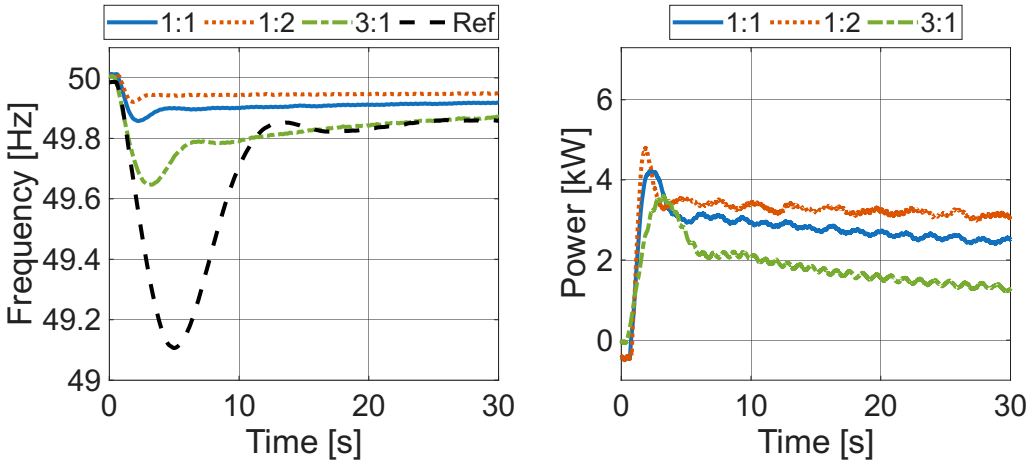

Figure 4.12: Grid frequency (left) and inverter power response (right) when both the inverter and the SG provide frequency regulation using the FCR-N controller. The inverter measures the frequency by the PLL and filters the signal with an LP filter with $\tau_{\mathrm{LP}} = 0.1$ s. The dashed line shows the frequency response when only the SG provides frequency regulation, used as the reference case. The solid, dotted and dash-dotted lines represent the inverter response with regulating strength equal to, twice or one-third of the SG, respectively.

In Fig. 4.12 the reference signal is the frequency response where only the SG does the frequency regulation and operates as an emulated hydro power plant. It can be seen that with the inverter operating with a third of the SG's regulating strength, the frequency nadir is significantly reduced compared to the reference. Furthermore when the inverter has twice the regulating strength of the SG, the frequency nadir is close to the steady-state level. Moreover, when operating with twice the regulating strength, the inverter is able to regulate most of the initial power imbalance before the SG has time to provide power. A larger regulating strength also requires more power during the steady state, since the inverter provides more power and reaches a smaller steady state error.

Operating the inverter with a generally low filtering time constant or without a filter on the measured frequency had a negligible difference from the response in Fig. 4.12. However, as the time constant increases, the inverter's power regulation slows down, resulting in a deeper frequency nadir. This can be seen in Fig. 4.13a where the filter time constant is increased from 0.1 s to 1 s and the inverter provides a third of the SG, the nadir drops below 49.6, compared to 49.65 Hz in Fig. 4.12.

Furthermore, a larger time constant led to a higher risk of instability, characterized by heavy oscillations in both frequency and power before settling. This is caused by the phase margin decreasing with an increasing time constant. To mitigate this, the 4/20 lead-lag filter is applied, which reduces the frequency of the oscillations, as presented in Fig. 4.13b.

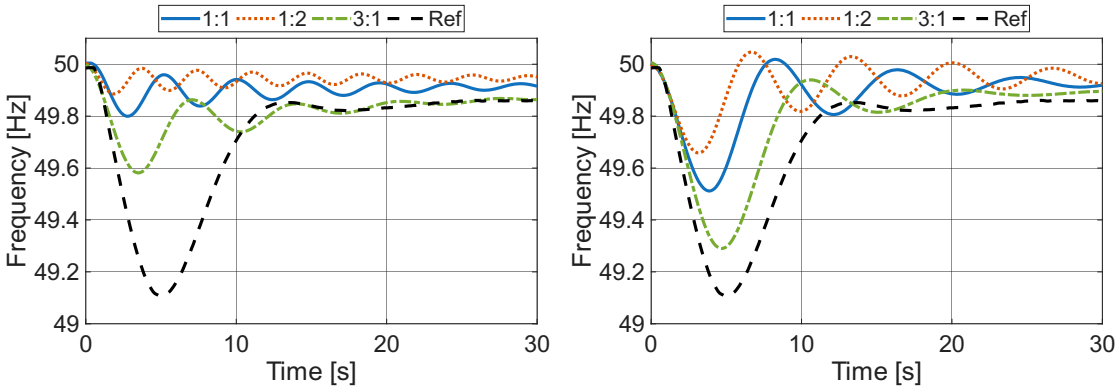

(a) With disabled 4/20 lead-lag filter. **(b)** With enabled 4/20 lead-lag filter.

Figure 4.13: Grid frequency response when both the inverter and the SG provide frequency regulation. The inverter measures the frequency by the PLL with an applied LP filter with $\tau_{\mathrm{LP}} = 1$ s on the frequency signal. The dashed line shows the frequency response when only the SG provides frequency regulation, used as the reference case. The solid, dotted and dash-dotted lines represents the inverter response with regulating strength equal to, twice or one-third of the SG, respectively.

As shown in Fig. 4.13a, low frequency oscillations were present before the 4/20 lead-lag filter was applied. At these lower frequencies, the filter's phase shift reduces the phase margin, which amplifies the oscillations as seen in Fig. 4.13b. The 4/20 lead-

lag filter's phase shift can be studied in Fig. 2.11. In contrast, with a MAVG filter with the same time constant of 1 s, the oscillations occur at higher frequencies. At these higher frequencies, the 4/20 lead-lag filter introduces less phase shift ,resulting in a larger phase margin. Consequently, the oscillations are effectively attenuated, improving stability, as shown in Fig. 4.14.

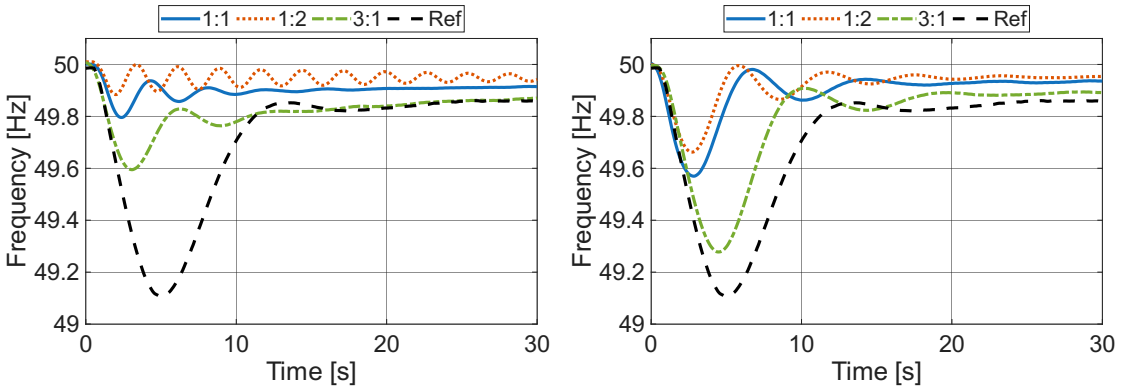

(a) With disabled 4/20 lead-lag filter. **(b)** With enabled 4/20 lead-lag filter.

Figure 4.14: Grid frequency response when both the inverter and the SG provide FCR-N. The inverter measures the frequency by the PLL with an applied MAVG filter with $\tau_{\text{MAVG}} = 1$ s on the frequency signal. The dashed line shows the frequency response when only the generator provides FCR-N, used as the reference case. The solid, dotted and dash-dotted lines represents the inverter response with regulating strength equal to, twice or one-third of the generator, respectively.

Comparing the oscillations in Fig. 4.14a with Fig. 4.13a, the frequency of the oscillation frequency has increased, and thus the lead-lag filter is more effective, as seen in Fig. 4.14b. A notable consequence of adding the 4/20 lead-lag filter is a deeper frequency nadir, since the lead-lag filter makes the inverter's response slower and smoother, as could be seen in Fig. 4.9. When the inverter operates with a regulating strength of a third of SG, the frequency nadir goes down to 49.3 Hz, which is close to the reference case. Therefore, there is a trade-off between reducing the frequency nadir or damping the amount of oscillations when implementing a lead-lag filter.

4.5 Dynamic FFR in Islanded Operation

The experiments with dynamic FFR, the same regulating strengths are used as for the measurements of shared frequency regulation, which is presented in Tab. 4.2. Furthermore, due to the similarity between the frequency filters (unfiltered, LP and MAVG), only the LP filter with a time constant of 0.1 s is evaluated. For the SG, it operates again as an emulated hydro power plant, which is used as the reference case and together with the inverter provides frequency regulation. With dynamic FFR the inverter should frequency regulate for the transient and fast changes in the frequency, then hand-over the frequency regulation to the SG which regulates

the frequency to a steady-state. Fig. 4.15 presents the inverter's response when the invert's regulating strength is equal (1:1), twice (1:2) and a third (3:1) of the SG's regulating strength, and when the HP filter has a time constant of 10 s.

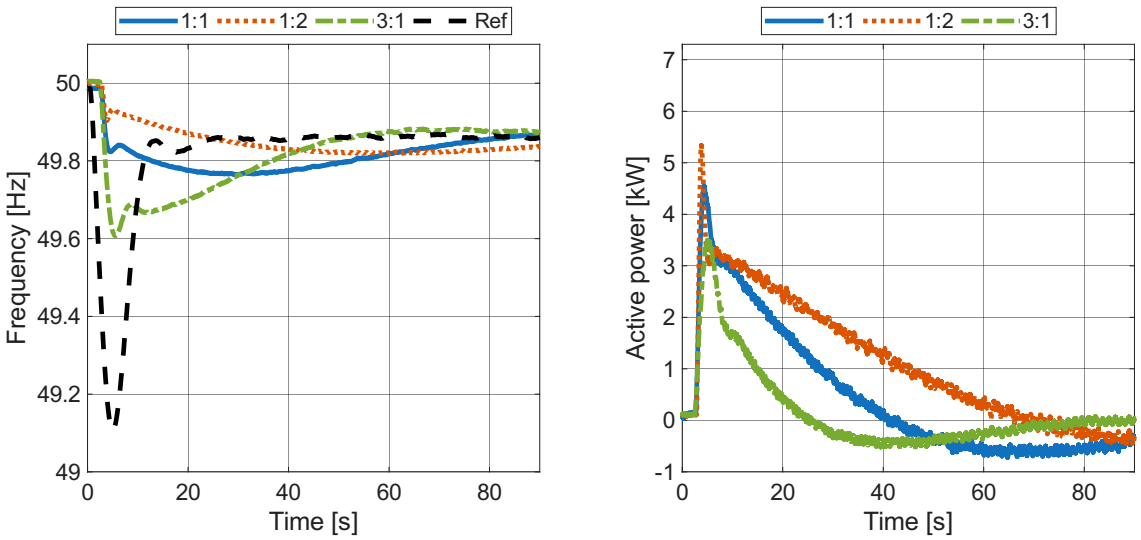

Figure 4.15: Dynamic FFR provision with a HP filter time constant of 10 s. The figure shows the measured frequency response (left) and active power injection (right) across the three SG-to-inverter strength ratios (1:1, 1:2, and 3:1, detailed in Tab. 4.2). The dashed line presents the reference case when only the SG provides frequency regulation.

From Fig. 4.15, the inverter is able to compensate for the initial and fast change in power demand and then hand over the regulation to the SG. This is seen by the high power peak at the 4.5 kW load step and then slowly ramping down the power output. This leads to the frequency nadir being smaller and the inverter only providing frequency regulation for fast changes and not steady-state errors. As shown in Fig. 4.16, increasing the HP filter time constant to 20 s, extends the frequency regulation handover period between the inverter and SG. This transition is characterized by a slower decline in power from the inverter than it was with a HP filter time constant of 10 s, as shown in 4.15.

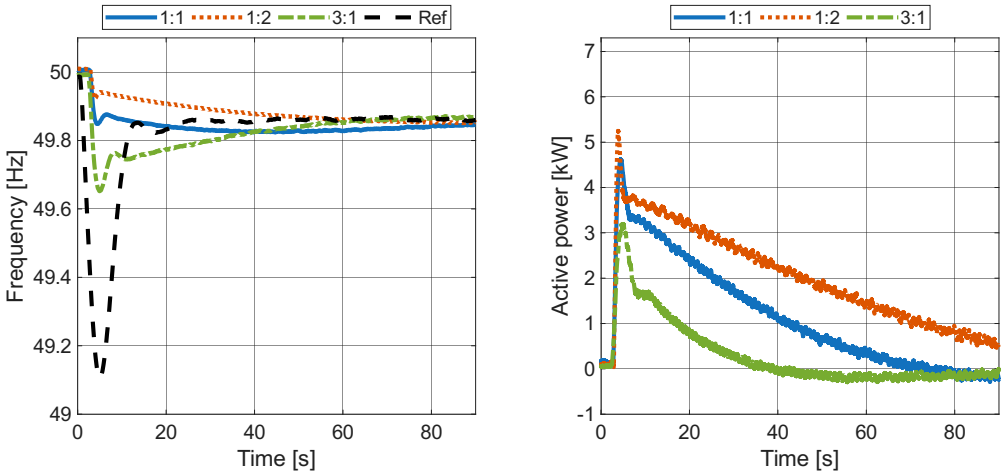

Figure 4.16: Dynamic FFR provision with a HP filter time constant of 20 s. The figure shows the measured frequency response (left) and active power injection (right) across the three SG-to-inverter strength ratios (1:1, 1:2, and 3:1). The dashed line presents the reference case when only the SG provides frequency regulation.

With a longer transition of frequency regulation from the inverter to SG, the overshoot in frequency when reaching steady-state is reduced. The overshoot difference in frequency is observed when comparing Fig 4.15 and 4.16, when the inverter having a regulating strength a third of the SG's. A higher HP filter time constant also results in the frequency nadir being improved upon, since both the initial nadir gets smaller and reduced overshoot at steady-sate. Increasing the HP filter time constant from 20 s to 60 s does not affect the lowest frequency nadir significantly, but the frequency regulation transition from the inverter to SG is so slow that there is no overshoot of the frequency when reaching steady-state. The result using a time constant of 60 s is presented in Fig. 4.17.

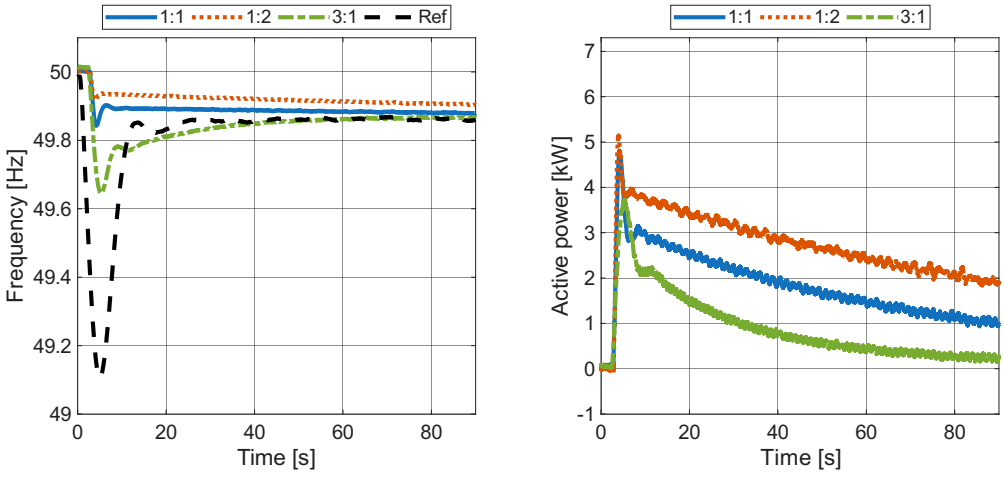

Figure 4.17: Dynamic FFR provision with a HP filter time constant of 60 s. The figure shows the measured frequency response (left) and active power injection (right) across the three SG-to-inverter strength ratios (1:1, 1:2, and 3:1). The dashed line presents the reference case when only the SG provides frequency regulation.

Comparing Fig. 4.17 to Fig. 4.15, the time it takes for the power output to reach zero takes much longer, but there is close to no overshoot in the frequency response. Using the external transducer for frequency measurements had an negligible effect on frequency and power response compared to using the PLL. The result of using an external transducer had a negligible affect on the power and frequency response. The main difference is an introduced transient peak in the power response, the frequency nadir was however unaffected.

Since the dynamic FFR controls the fast changes and the SG handles the hand-over and steady state frequency regulation, the regulation of the SG's turbine becomes smoother and slower. The dynamic response of the SG turbine and the inverter is presented in Fig. 4.18. The measurements show the case where the inverter has a regulating strength of a third (3:1) of the SG's and an HP filter time constant of 20 s.

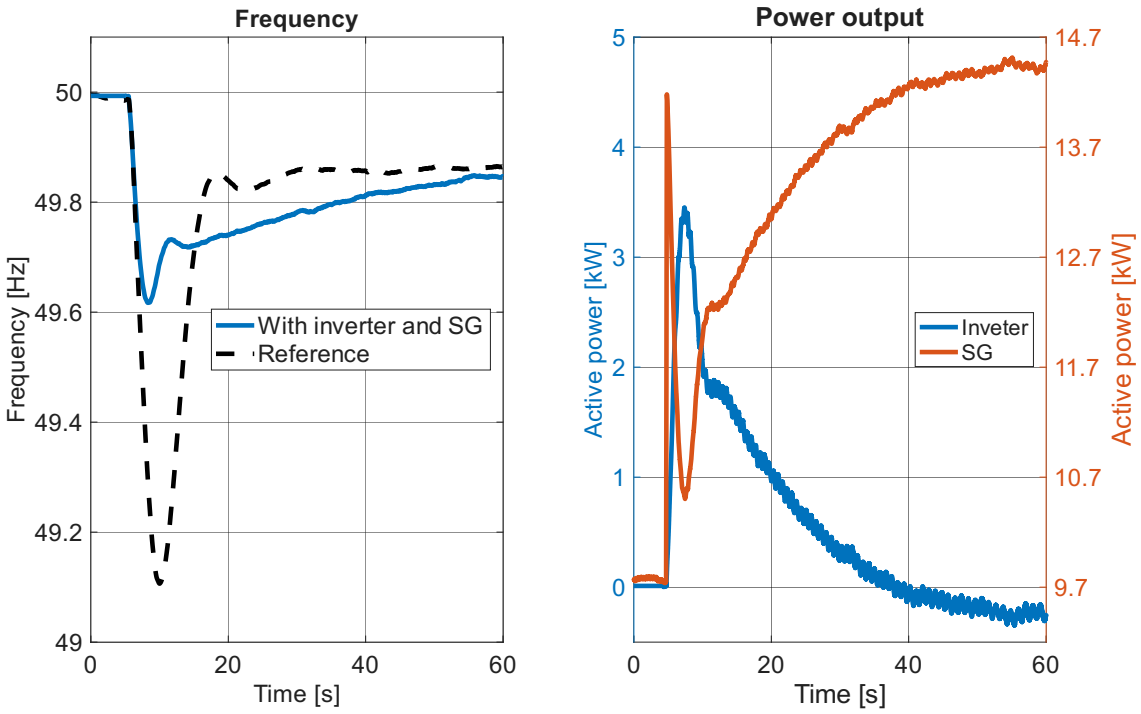

Figure 4.18: Dynamic FFR provision with HP filter time constant of 20 s and a regulating strength equal to a third of the SG. The figure shows the frequency response on the left, both with and without the inverter enabled. The tight figure presents the active power injection from both the SG and inverter. The inverter operates with a regulating strength equal to a third of the SG.

As seen in Fig. 4.18, the initial output power comes from the inertia response of the SG. However, afterward, the SG gradually ramps up its power output to the desired level. Furthermore, since the SG could increase its power output more smoothly to the desired power level, the wear and tear on the turbine and valves of the power plant could potentially be reduced. This means that variation in mechanical movements is reduced and smoothed out.

Furthermore, from Fig. 4.15-4.17 it could be observed that with a higher time constant on the HP filter, the time it took for the hand-over of frequency regulation from the inverter to the SG increased, since it took longer for the inverter to return to 0 kW. This allows the SG to achieve steady-state in a slower and smoother response with a higher HP filter time constant, thus further reducing deterioration.

4.6 Synthetic Inertia in Grid-Connected Operation

To evaluate synthetic inertia, a simulated ramp is applied on the measured frequency. Depending on the synthetic inertia constant, the ramp is tuned such that power never exceeds its rating, and the maximum frequency ramp is 2 Hz/s. Furthermore, as seen in Section 4.1, MAVG filtered has lower stability margins than unfiltered and LP filtered, thus, MAVG was neglected. Fig. 4.19 shows the frequency signal and power response for an example case with an inertia constant of 25 s and ramp of 0.9 Hz/s. The test sequence consists of the frequency ramp applied for 5 s, followed by a 5 s period of constant frequency and a final 5 s negative ramp to restore frequency to its nominal value.

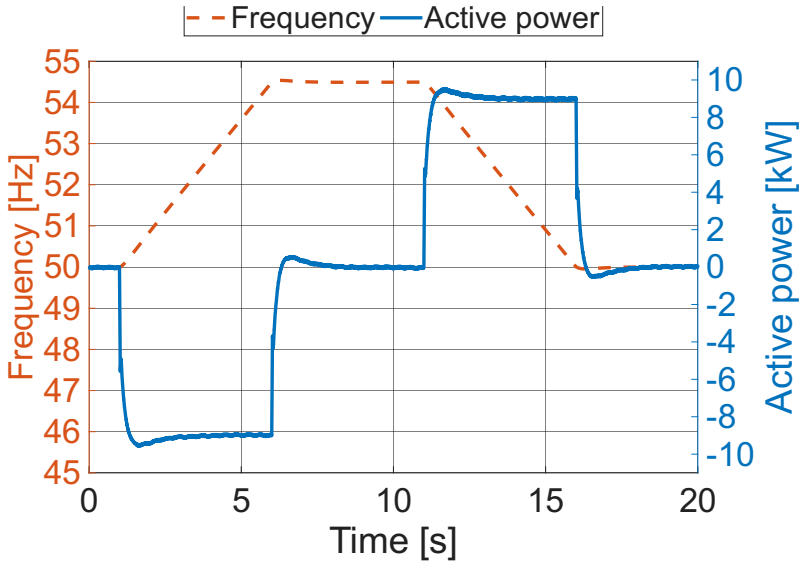

Figure 4.19: Inverter power response (solid line) to a three-stage frequency cycle (dashed line) under weak grid conditions, a inertia constant of 25 s, a LP frequency filter with 0.7 s time constant and frequency measured with the PLL. The frequency cycle includes a 0.9 Hz/s ramp for 5 s, a constant frequency for 5 s and a negative recovery ramp for 5 s.

The result presented in Fig. 4.19 shows an example of a stable response, indicated by a small overshoot and small oscillations at steady state. For the shown example case, frequency is taken from the PLL and filtered through an LP filter with a time constant of 0.7 s.

If the simulated ramp where to progress over a longer period the inverter is able to produce the equivalent power of the ramp and inertia constant. However, if the ramp were to happen in the actual frequency, the assumption that the inverter operates around a 50 Hz would be invalid and thus could lead to the inverter malfunction. If the ramp were however to increase the inverter could be saturated and limited to deliver only the rated power.

To evaluate the maximum inertia constant, the same test cycle is used, but with the ramp adapted to the inertia constant so the output power does not exceed the rated power of the inverter. For the cases with unfiltered frequency, the noise of the grid frequency saturated the inverter control. This introduced significant uncertainties for the maximal inertia constant for both the PLL and the externally measured frequency. With the LP filter, the noise was reduced and the maximum inertia constants could be evaluated, presented in Fig. 4.20.

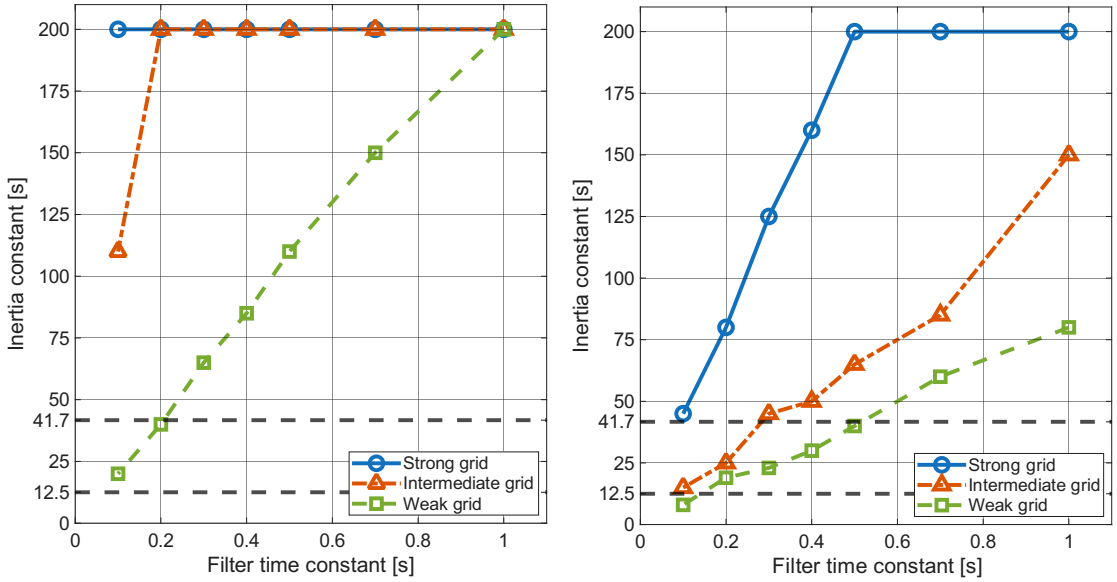

(a) Measuring the frequency by the PLL

(b) Measuring the frequency by the external transducer

Figure 4.20: The maximum inertia constant in a strong, intermediate and weak grid as a function of the frequency LP filtering time constant for different methods of measuring frequency. The lower horizontal dashed line indicate the targeted inertia constant of 12.5 s. As reference the SG had a inertia constant of 41.7 s referred to the inverter's base, which is the upper horizontal dashed line.

As shown in Fig. 4.20, the majority of tests points yield a synthetic inertia constant exceeding that of the SG. This indicates that the inverter is able to strengthen the grid's frequency stability to a degree similar to or beyond that of the SG, since a higher inertia constant implies a stiffer grid with a lower RoCoF. Therefore, synthetic inertia could be a great option to use as converted-based production units increases.

As seen in Fig. 4.20b, synthetic inertia is very sensitive to low filtering time constants for the external transducer, compared with the use of PLL, presented in Fig 4.20a. This is due to the time delay and possible phase shift of the external transducer that shifts the response of the inverter in regard to frequency. Furthermore, the stability of the inverter is highly dependent on the strength of the grid, since a weak grid performs significantly worse than a strong grid.

4.7 Comparison Between Synthetic Inertia and Dynamic FFR in Islanded Operation

Both synthetic inertia and dynamic FFR focus on the initial fast transient following a frequency disturbance. Since they share the same objective, this section presents a comparison of the effectiveness of the two controllers. However, since a stability analysis regarding maximum regulating strength for dynamic FFR were not conducted, the performance of reducing the frequency nadir is compared. The comparison was made in island operation, where the 4.5 kW load is switched in. The SG operates as a hydro power plant and is used as a reference frequency response. For an even comparison between these two, the peak power was tuned to be the same by tuning the regulating strength and the inertia constant. The regulating strength and inertia constant to achieve a power peak of 3 kW when performing a 4.5 kW step load are presented in Tab. 4.3.

Table 4.3: Regulating strength and inertia constant to compare the performance of dynamic FFR and synthetic inertia, respectively. The regulating strength and inertia constant are tuned for each filter type and time constant, such that the peak of the power response is 3 kW.

Frequency filtering	HP filter time constant [s]	Regulating strength [p.u./p.u.]	Regulating strength [kW/Hz]	Inertia constant [s]
PLL - 0.1 s	10	160	32	70
	20	165	33	
	60	166	33.2	
PLL - 1 s	10	35	7	80
	20	30	6	
	60	25	5	
External - 1 s	10	34	6.8	68
	20	29	5.8	
	60	27	5.4	

With the tuned regulating strength and inertia from Tab. 4.3, the power response for 4.5 kW load step is compared for synthetic inertia and dynamic FFR. While dynamic FFR is evaluated using a HP filter time constant of 10, 20, 60 s, Fig. 4.21 shows the comparison using the 20 s setup to illustrate the differences between the two frequency ancillary services.

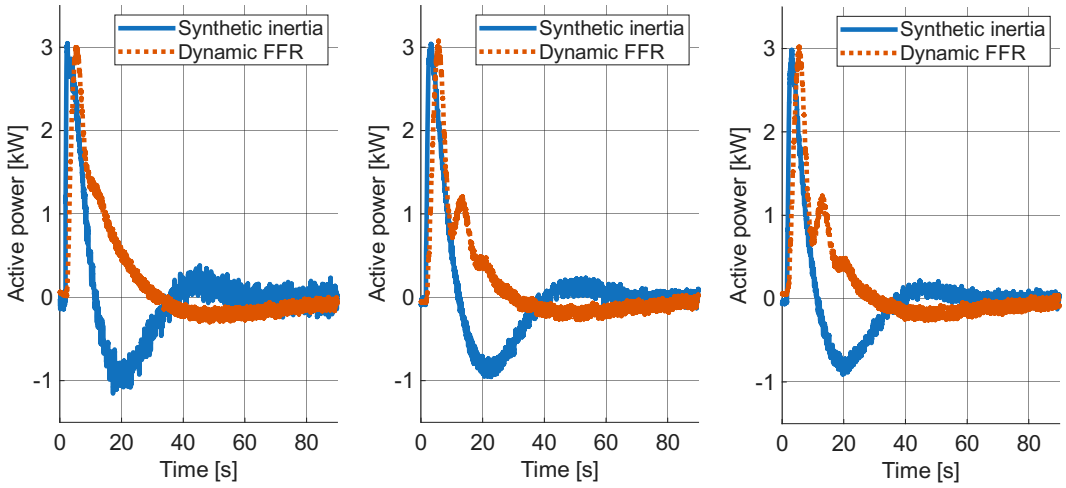

(a) PLL-based frequency measurement, filtered by a LP filter with a time constant of 0.1 s.

(b) PLL-based frequency measurement, filtered by a LP filter with a time constant of 1 s.

(c) External transducer-based frequency measurement, filtered by a LP filter with a time constant of 1 s.

Figure 4.21: Comparison between the inverter's power injection when comparing synthetic inertia against dynamic FFR, for different filtering time constant and with PLL or the external transducer for frequency measurements. The dynamic FFR has a HP filter with $\tau_{\mathrm{HP}} = 20$ s.

Fig. 4.21 presents the result when using the LP filter with a time constants of 0.1 s and 1 s when measuring the frequency by the PLL, and the result from using the external transducer with a 1 s LP filter. However, with a time constant of 0.1 s with the external transducer, the synthetic inertia did not reach a peak of 3 kW without being unstable. This could be seen by Tab. 4.3 and Fig. 4.20b, as the necessary inertia constant would be around 70 s, and assuming island operation has similar limits to a strong grid-connection operation, the necessary inertia constant would exceed the stability limits.

From Fig. 4.21, it is shown that the response of the synthetic inertia controller is faster than dynamic FFR, since synthetic inertia reaches its peak earlier. This is due to the synthetic inertia controller being less filtered than the dynamic FFR controller and regulates against the frequency derivative, instead of the frequency deviation. However, the dynamic FFR has a more damped frequency response, without any overshoot. The synthetic inertia has an overshoot in frequency when reaching steady-state at around 40 s which is seen in the corresponding frequency response to the power response is presented in Fig. 4.22.

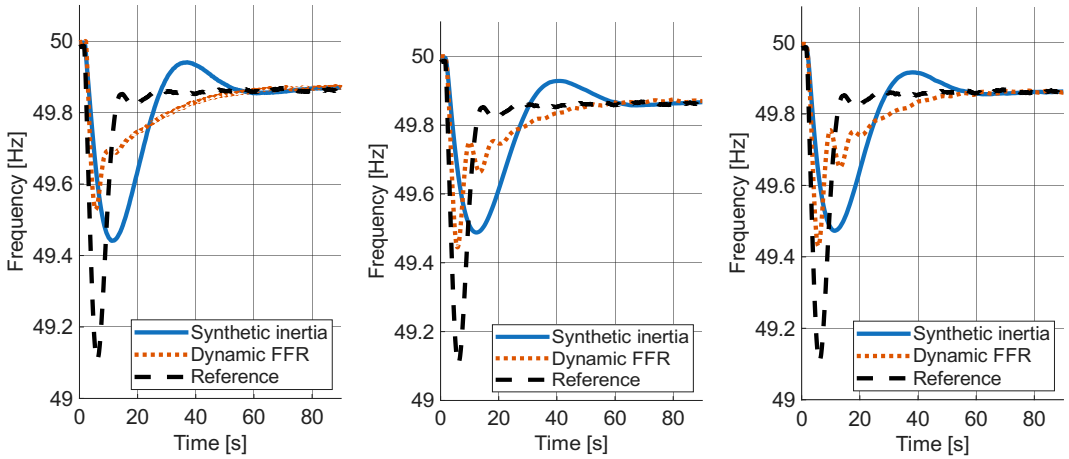

(a) PLL-based frequency measurement, filtered by a LP filter with a time constant of 0.1 s.

(b) PLL-based frequency measurement, filtered by a LP filter with a time constant of 1 s.

(c) External transducer-based frequency measurement, filtered by a LP filter with a time constant of 1 s.

Figure 4.22: Comparison between the grids frequency when comparing synthetic inertia against dynamic FFR, for different filtering time constant and with PLL or the external transducer for frequency measurements. Where the dotted line represent when the inverter frequency regulate with dynamic FFR, the synthetic inertia regulation is shown by the solid line and the dashed line present the reference case were the inverter is disconnected. The dynamic FFR has a HP filter with $\tau_{\mathrm{HP}} = 20$ s.

With either dynamic FFR or synthetic inertia, the frequency nadir is improved compared to the reference. It is seen that for an LP filter time constant of 1 s, in Fig. 4.22b and 4.22c, the frequency nadir with synthetic inertia is smaller than that of the dynamic FFR. However, for a time constant of 0.1 s, Fig. 4.22a, the dynamic FFR performs better, seen from the frequency nadir. The reason why synthetic inertia performs better at higher filtering time constants than dynamic FFR is because of how it affects the measured frequency. The dynamic FFR controller regulates depending on the frequency deviation, and with more filtering, the measured deviation increases more slowly, thus reducing the effectiveness. However, synthetic inertia regulates on the frequency derivative and with low filtering time constant the signal is quite noisy, making the derivative and consequently the reference power increasing and decreasing rapidly. Therefore, with higher filtering time constants, the derivative becomes more steady, since the measured frequency increases without much noise, which would otherwise affected the derivative. Hence, the synthetic inertia performs better with higher filtering time constants and dynamic FFR for lower filter time constants.

In addition to comparing the frequency nadirs, the maximum amount of energy needed for each case is compared in Tab. 4.4. As described in Section 3.4.2, the calculated power is passed through a 50 Hz LP filter. The maximum energy capacity

is found by integrating the output power, starting when the 4.5 kW load is connected until the power response reaches the first zero-crossing. Therefore, maximum energy integration does not consider power after the polarity of the power output has been changed.

Table 4.4: Compilation of the required energy, lowest frequency nadir and initial RoCoF for synthetic inertia and dynamic FFR, with the maximum power peak tuned to 3 kW as presented in Tab. 4.3. The table includes result for both the PLL and external frequency measurement, LP filtering time constants 0.1 s and 1 s, and the HP time constants used for the dynamic FFR.

Frequency filtering	HP time constant [s]	Maximum energy [kJ]		Frequency nadir [Hz]		Initial RoCoF [Hz/s]	
		Synthetic inertia	Dynamic FFR	Synthetic inertia	Dynamic FFR	Synthetic inertia	Dynamic FFR
PLL 0.1 s	10	15	23	49.44	49.54	-0.094	-0.19
	20		28		49.53		-0.20
	60		49		49.50		-0.21
PLL 1 s	10	16	19	49.49	49.47	-0.065	-0.091
	20		24		49.45		-0.094
	60		44		49.41		-0.090
External 1 s	10	14	19	49.47	49.45	-0.066	-0.082
	20		23		49.43		-0.086
	60		40		49.43		-0.087

As seen in Tab. 4.4, the least energy storage capacity is needed for synthetic inertia for all cases. Furthermore, it is shown that a higher HP filter time constant increases the necessary energy storage capacity, and the frequency nadir gets slightly worse. The increase of energy storage capacity for dynamic FFR for higher HP filter time constants is due to the longer hand-over between the inverter and SG. For dynamic FFR this hand-over process can be regulated by the HP filter time constant, while for synthetic inertia the hand-over process is not controlled.

In Tab. 4.4 is the initial RoCoF also presented, which is calculated by the derivative of the change in frequency from when the 4.5 kW load is connected and one second forward. For the reference case, with only the SG connected, the initial RoCoF was -0.23 Hz/s. When comparing the reference case with dynamic FFR, with a frequency filter time constant of 0.1 s the dynamic FFR does not improve the RoCoF significantly. Increasing the HP filter time constant did, in most cases, worsen the RoCoF because the HP filter then includes slow changes. Since the regulating strength was tuned to achieve a peak of 3 kW, which is dependent on slower changes, the dynamic FFR becomes less aggressive for fast frequency changes. Increasing the LP filter time constant improves the RoCoF instead, as the measurements become less noisy, making the measured change increase more steadily. This results in the inverter delivering a steadier output power.

Synthetic inertia is, however, more effective in reducing the RoCoF and becomes

even more effective at a higher frequency filtering time constant because the filtering reduces measurement noise. The inverter estimates the RoCoF using a discrete momentary derivative, calculated as the difference between the current and previous samples divided by the sampling time. Without sufficient filtering, this derivative significantly amplifies high-frequency noise, leading to heavily distorted reference signals for the inverter. Conversely, with a higher filtering time constant the calculated RoCoF becomes more stable resulting in the reference signal becoming less noisy. If the reference signal is very noisy the inverter has to constantly and rapidly change its output level, which affects the measurement as well, leading to a noisier signal.

The comparison between dynamic FFR and synthetic inertia shows that the most suitable frequency ancillary service may depend on requirements and system conditions. Synthetic inertia could be preferred when a fast response is required, while dynamic FFR may be more advantageous for applications that require a more damped and stable frequency response. In the future, a combination of these systems could be used to provide fast and stable frequency support for low-inertia systems, while also enabling the frequency containment reserves (FCR) to respond effectively.

5

Discussion of Inverter Tuning for Stability and a Comparison of FCR-N and Dynamic FFR Regulation

This chapter first discusses the implementation of FCR-N operation in both islanded and grid-connected operation with the impact of the tuning of filter parameters. The tuning of these parameters focused on achieving high stability margins in regulating strength while operating with different grid strengths for grid-connected operation, as well as in islanded operation. The implementation discussion focused on the implication of high margins in regulating strength and the operation of the two power controllers, PC-PI and PC-DIV. A comparison between dynamic FFR and FCR-N regulation is thereafter presented. The final sections of this chapter present a discussion of societal and ecological aspects, followed by a discussion of future work.

5.1 Tuning of Frequency Filter for Stability with FCR-N

This section discusses the choice of filtering parameters and measuring method for frequency measurement while considering the stability margins of the inverter. The stability margins were evaluated for FCR-N operating in grid-connected mode or islanded operation. The aim was to achieve a stable operation at a regulating strength of 500 p.u./p.u. (100 kW/Hz) or above. A higher regulating strength than 500 p.u./p.u. (100 kW/Hz) was desirable, as it created a stability margin. Operating with very small margins increases the risk of instability caused by variations in the grid or inverter parameters. Therefore, maintaining sufficient stability margins is important for robust inverter operation.

As seen from the stability analysis for grid-connected operation in Fig. 4.2, 4.3 and for islanded operation in Fig. 4.10 the first order LP filter provided the overall highest stability margins, from 500 p.u./p.u. (100 kW/Hz). This was achieved

independently of any combinations of grid strength, voltage source, type of power controller or frequency measurement device. In addition to the LP filter being the preferred filtering method, measuring the frequency via a PLL yielded a stable regulating strength higher than that of the external transducer. There are some exceptions where the LP or PLL had lower stability margins than other combinations, however for the majority of cases, the LP filter and measuring frequency by the PLL had highest stability margins. Operating with small margins increases the risk of instability caused by variations in the grid. Therefore, maintaining sufficient margins is essential for robust inverter operation. If the 4/20 lead-lag filter was applied, the LP filter and PLL measurement reached the maximum regulating strength used (1000 p.u./p.u. or 200 kW/Hz) for all combinations, demonstrating a substantial stability margin. Therefore, in terms of the stability margins for regulating strength, the combination of a PLL and LP filter appeared to be the most effective.

When tuning the filter time constant, one option is to use only the LP filter with the PLL since it was stable in all tests during islanded operation. Therefore, the regulating strength has to be tuned only after the grid-connected operation, since the maximum stable regulating strength varied with the filtering time constant. However, excluding all other filter combinations is quite restrictive. Rather than compromising between filter methods, the filter parameters could be tuned to achieve the most versatile inverter. To do this, the parameters should be tuned for the two worst cases that in general resulted in the lowest stability margins, which were weak grid in grid-connected operation and islanded operation. Tuning the filter based on these worst cases creates more flexibility in choosing filters and increases the regulating strength margin from instability.

If the priority instead is to not achieve full versatility, but rather tune specifically for stronger grids that are less prone to instability, the filter time constants can be tuned based on the stability limits for intermediate and strong grids presented in Fig. 4.3. When considering both the PLL and the external transducer, the minimum filter time constant was found to be 0.1 s for the LP filter and 0.4 s for the MAVG filter. For weak grids and islanded operation, the tuning should combine the results of weak grids (Fig. 4.2) and island operation (Fig. 4.10). The minimum filter time constant to achieve a regulating strength of 500 p.u./p.u. (100 kW/Hz) was found to be 0.2 s for the LP filter and for the MAVG filter it was 0.4 s. However, as presented in Section 4.3, a too high filter time constant leads to instability. Therefore, a time constant of around 0.3-0.7 s for the LP filter and 0.5 s for the MAVG filter is appropriate for ensuring stability.

A third option is to implement the lead-lag filter. With the 4/20 lead-lag filter, the regulating strength achieved 1000 p.u./p.u. (200 kW/Hz) for the majority of cases, the few that did not reach it were close. By implementing the lead-lag filter, existing GFL inverter's could operate on the FCR-N market with high regulating strength without replacing existing hardware or extensive tuning of filtering time constants. The drawback of the lead-lag filter is the slower response time, which increases the frequency nadir, as indicated in Fig. 4.14b.

5.2 Influence of Regulating Strength and Power Controller on the Stability of an Inverter While Providing FCR-N

Although the two power controllers (PC-PI and PC-DIV) were tuned according to the same procedure, the PC-PI by its PI regulator, and the simplified PC-DIV by its LP filter, their resulting time constants differed. Therefore, a fair comparison between the power controllers cannot be conducted on a detailed level. However, the results show that the power controllers yielded a similar maximum regulating strength. Furthermore, based on the results of the technical requirements tests for FCR-N, the differences between the power controllers had a negligible effect on the technical requirements. Given these similar results in regulating strength and requirements, the simplification of the PC-DIV did not significantly affect the inverter's performance. Therefore, for experiments with dynamic FFR and synthetic inertia, it was assumed that PC-DIV and PC-PI would yield a similar outcome.

One advantage of PC-DIV over PC-PI is that no integrator is needed. Without the integrator, the risk of integrator wind-up is eliminated, and the overall calculations are less demanding. Furthermore, a second advantage is that less tuning is needed for the PC-DIV. The PC-PI is tuned by K_{I} and K_{P}, which determine the characteristics of the response. For the PC-DIV, only the LP filter's time constant is tuned. This simplifies implementation and if future tuning is desired, only one parameter has to be changed. However, a drawback of the PC-DIV is that division by zero could occur, by voltage dips in weak grid or disturbances in the measurements, leading to a high reference current. However, this is compensated for by the saturation block in the power controller that limits the reference current, $I_{\mathrm{ref}}^{\mathrm{d}}$, to a maximum of 1.11 p.u.

5.3 Comparison between Dynamic FFR and FCR-N for Frequency Regulation

As previously shown, the inverter has a fast power response following a frequency deviation. Therefore, the idea of using the inverter to provide dynamic FFR, which takes care of only the initial fast and severe frequency deviations, seemed advantageous. Comparing the frequency nadir between the dynamic FFR in Fig. 4.12 and the FCR-N provision in Fig. 4.15-4.17 the frequency nadir is unchanged or slightly reduced, for equal regulating strength and the same frequency filter. However, since the reserve is active for a shorter period of time, the amount of energy consumed is also reduced, which is important to consider if a limited energy reservoir were to be used. Therefore, a higher regulating strength could be utilized to decrease the frequency nadir without exceeding the energy required for FCR-N.

5.4 Societal and Ecological Aspects

As the share of renewable inverter-based sources increases in the grid, the reliance on conventional generators which is driven by fossil fuel is reduced. This transition decrease the greenhouse gas emissions from electricity production. However, the technologies for renewable sources such as solar cells, wind parks, batteries and inverters all require a high amount of raw materials and energy during manufacturing. Furthermore, the extraction, manufacturing and transport causes environmental damages and emissions. These effects can be reduced by using renewable energy in the production and develop more environmental friendly materials and manufacturing methods.

An ethical and geopolitical concern is the origin of the materials used in renewable energy technologies. Many of these materials, including cobalt, lithium and rare earth elements, are extracted in countries such as the Democratic Republic of the Congo [41]. The study further reports concerns about poor working conditions, the risk of child labor and limited protection for the workers mining these materials. To be dependent on a small number of countries for critical materials could also create geopolitical vulnerabilities and logistical risks. Ensuring transparent supply chains, improving labor standards and increasing material recycling could help reduce these ethical and geopolitical concerns.

The implementation of frequency ancillary services through inverters could influence the societal perception of renewable energy, if these services are seen as helping to address the challenges with integrating a larger share of renewable resources. There are several barriers to deploy renewable energy systems as a reliable power source, these are identified in [42] and includes intermittency and forecasting difficulties. Furthermore, research on public opinion shows that many people still perceive renewable energy sources as unstable and less reliable than conventional generation. For example, [43] reports that Americans generally view solar and wind power as less reliable than other energy sources. By improving grid support and system stability, frequency ancillary services provided by inverter-based sources may therefore address both the technical and societal barriers to the renewable energy adaptation.

One other important aspect to consider is the security of inverters, which consists of power electronics with digital controllers. In setups such as the one used in this thesis, vulnerabilities to cyberattacks may arise, where an attacker could gain access to the control system and intentionally destabilize the system. To prevent unauthorized access, security systems must be implemented to mitigate vulnerabilities.

6

Conclusion and Future Work

The aim of this thesis was to analyze the stability and performance of a GFL inverter when providing frequency regulation. The stability limits for FCR-N and synthetic inertia were evaluated. The stability limits of the inverter were analyzed either in grid-connected operation, when connected to the local power grid, or in islanded operation with a synchronous generator. For grid-connected operation, the stability was evaluated with a weak, intermediate or strong grid. The inverter's stability limits were determined by finding the maximum achievable regulating strength or inertia constant before reaching instability. The FCR-N regulation was also assessed against the technical requirements for FCR defined by ENTSO-E. Performance was then evaluated using the same setup, with either in grid-connected or islanded operation. The impact of the frequency measurement method, frequency filter and filter time constant was evaluated to determine the inverter's stability and performance.

For FCR-N operation, it was found that the stability limits regarding regulating strength had large margins from the desired strength of 500 p.u./p.u. in most cases. In weak grids and islanded operation, however, the desired regulating strength was not always achieved or margins were small. The minimum filter time constant to achieve 500 p.u/p.u. for all was 0.2 for the LP filter and 0.4 s for the MAVG filter. The result showed that the external frequency transducer performed worse for all combinations, and for grid-connected operation, a lower filtering time constant reduced the maximum regulation strength.

For islanded operation, with the inverter utilizing the FCR-N controller, both high and low filtering time constants reduced the regulating strength. This reduction occurred since lower time constants did not attenuate high-frequency noise but increased the phase shift, whereas higher time constants introduced significant delays that reduced the phase margins. To improve the stability limits, a lead-lag filer could be implemented, resulting in almost all combinations reaching 1000 p.u./p.u. (200 kW/Hz) However, the drawback is an increased response time that leads to a deeper frequency nadir. Evaluating against the technical requirements for FCR, it was found that the inverter fulfilled the requirements well within limits.

The inverter's FCR-N operation was thereafter evaluated in island operation without the SG providing any frequency regulation. The result showed that the inverter could regulate the frequency for both the grid between the inverter, the load and the SG.

Lastly, the frequency regulation in the SG was reinstated. The result showed that the inverter and SG could share the frequency regulation and that with an inverter the frequency nadir could be reduced in comparison when only the SG provided frequency support.

The FCR-N controller was thereafter equipped with an HP filter, converting the controller into dynamic FFR. The performance of dynamic FFR was evaluated in islanded operation and showed a remarkable improvement in frequency nadir compared to when only the SG did the frequency regulation. The time constant of the HP filter determined how fast the SG should take over frequency regulation from the inverter responsibility. Furthermore, since the inverter provides faster frequency regulation than the SG, the inverter could manage the faster transients, allowing the SG to operate more smoothly and against slower variations.

Lastly, the result for the inverter stability limits during operation with synthetic inertia showed reduced stability at lower filtering time constants. The maximum achieved emulated inertia constant of the inverter was for many cases above the SG's inertia (normalized to the inverters base). Indicating the inverter's potential to operate similarly to a SG, even without a rotating mass. Comparison between dynamic FFR and synthetic inertia showed that, for the same power peak, dynamic FFR provided a faster response to frequency variation and reduced the frequency nadir more. However, due to its higher energy demand, a trade-off between available energy capacity and the desired frequency nadir must be considered when selecting the appropriate service.

6.1 Future Work

It can be noted that the technical requirements for FCR-N were well fulfilled, suggesting that different requirements could be developed and performed to better utilize the inverter's fast response time. Furthermore, both dynamic FFR and synthetic inertia showed promising results for fast frequency regulation. Therefore, to enable their operation in the frequency regulation market, market frameworks and financial incentives for dynamic FFR and synthetic inertia need to be developed. To achieve this, introducing market-based frequency ancillary services would allow producers to voluntarily provide synthetic inertia based on unit capacity, grid needs and financial compensation. A next step could be to study the new requirements that could be used for inverter based frequency regulation. Furthermore, the limitations for synthetic inertia in island operations were not evaluated in this thesis, but could be studied as well.

Further tuning of the PC-PI and PC-DIV could be performed to investigate how a faster or slower power controller could impact the results. For the PC-PI, this includes tuning of the proportional and integral gain and for the PC-DIV only the LP filter has to be tuned, since the LP filter regulates the PC-DIV's response. Investigating how fast the power controller response can be while still maintaining the system stable when regulating frequency regulating against either the grid or the

SG is of interest. A faster power response would improve the speed of the frequency support, thereby counteracting frequency deviation faster.

In this thesis, only one frequency ancillary service has been used at a time, but combinations of multiple frequency ancillary services could be implemented. Other functionalities could be investigated, such as adding a voltage controller to the inverter. Since weak grids can suffer from large voltage variations, adding a voltage regulator could help manage overvoltage or undervoltage by injecting or absorbing reactive power. Therefore, future work could investigate how an inverter with an integrated voltage regulator impacts grid stability, since this function was provided by the external grid or an SG in this thesis.

To further improve stability in weak grids, future work could evaluate the same experiments performed in this thesis using a GFM inverter. This is because GFL inverters depend on a PLL, which increases their sensitivity to instability in weaker grids. Investigating the behavior of a GFM inverter would provide a foundation for how inverter-based resources can support voltage and frequency regulation in future grids.

Based on the findings from the experiments in the power system laboratory, future research could expand from a controlled network model to large-scale implementations. This expansion is necessary to investigate the interactions between multiple inverters and control stability in more complex networks. Furthermore, integrating the developed control structure with battery energy storage systems or hybrid power plants could show how to coordinate and manage inverter-based resources in practical applications.

Bibliography

[1] International Renewable Energy Agency, "Renewable capacity statistics 2025," International Renewable Energy Agency, Abu Dhabi, Report, 2025. [Online]. Available: https://www.irena.org/Publications/2025/Mar/Renewable-energy-statistics-2025.

[2] *Om olika reserver*, sv, Oct. 2025. Accessed: Jan. 23, 2026. [Online]. Available: https://www.svk.se/aktorsportalen/bidra-med-reserver/om-olika-reserver/.

[3] Z. Mirza and H. Jain, "From challenges to solutions: Review and analysis of grid-supportive technologies in sustainable power systems," *Applied Energy*, vol. 403, p. 127 111, 2026, ISSN: 0306-2619. DOI: https://doi.org/10.1016/j.apenergy.2025.127111. [Online]. Available: https://www.sciencedirect.com/science/article/pii/S0306261925018410.

[4] D. Fernández-Muñoz, J. I. Pérez-Díaz, I. Guisández, M. Chazarra, and Á. Fernández-Espina, "Fast frequency control ancillary services: An international review," *Renewable and Sustainable Energy Reviews*, vol. 120, p. 109 662, 2020, ISSN: 1364-0321. DOI: https://doi.org/10.1016/j.rser.2019.109662. [Online]. Available: https://www.sciencedirect.com/science/article/pii/S1364032119308676.

[5] Q. Zong, W. Yao, H. Zhou, Y. Xiong, W. Gan, and J. Wen, "Hierarchical optimal frequency support scheme of wind farm with both grid-forming and grid-following wind turbines," *International Journal of Electrical Power & Energy Systems*, vol. 165, p. 110 463, 2025, ISSN: 0142-0615. DOI: https://doi.org/10.1016/j.ijepes.2025.110463. [Online]. Available: https://www.sciencedirect.com/science/article/pii/S0142061525000146.

[6] M. K. Khan, K. Kauhaniemi, H. Laaksonen, and M. A. Hassan, "Review of recent developments in grid codes: Focus on compliance testing and grid-forming inverter-based resources," *Renewable and Sustainable Energy Reviews*, vol. 227, p. 116 509, 2026, ISSN: 1364-0321. DOI: https://doi.org/10.1016/j.rser.2025.116509. [Online]. Available: https://www.sciencedirect.com/science/article/pii/S1364032125011827.

[7] R. Aljarrah, B. B. Fawaz, Q. Salem, M. Karimi, H. Marzooghi, and R. Azizipanah-Abarghooee, "Issues and challenges of grid-following converters interfacing renewable energy sources in low inertia systems: A review," *IEEE Access*, vol. 12, pp. 5534–5561, 2024. DOI: 10.1109/ACCESS.2024.3349630.

[8] Svenska kraftnät, "Förkvalificering," Dec. 2025. Accessed: Jan. 22, 2026. [Online]. Available: https://www.svk.se/aktorsportalen/bidra-med-reserver/forkvalificering/.

[9] Federal Ministry for Economic Affairs and Climate Action (BMWK), *Now available on the market: Instantaneous reserve through renewables and storage system*, Accessed: May 2026, Feb. 2026. [Online]. Available: https://energiewende.bundeswirtschaftsministerium.de/EWD/Redaktion/EN/Newsletter/2026/02/Meldung/news2.html.

[10] A. Karlsson and C.-J. Vickström, "Implementation and Stability Analysis of Synthetic Inertia for Inverter-Based Energy Resources," eng, 2025. Accessed: Feb. 20, 2026. [Online]. Available: https://odr.chalmers.se/items/1d33cfe3-f867-4250-b7da-f58ae3e25217.

[11] ENTSO-E, *Technical Requirements for Frequency Containment Reserve Provision in the Nordic Synchronous Area*, Brussels, Belgium. Accessed: Feb. 20, 2026. [Online]. Available: https://www.svk.se/495d28/siteassets/aktorsportalen/bidra-med-reserver/om-olika-reserver/fcr/fcr-technical-requirements_v1.1_28_march_2025.pdf.

[12] M. Nagaboopathy, K. D. R. Pandu, A. Selvaraj, and A. S. Velu, "Improved fault resilience of gfm-gfl converters in ultra-weak grids using active disturbance rejection control and virtual inertia control," *Sustainability*, vol. 17, no. 14, 2025, ISSN: 2071-1050. DOI: 10.3390/su17146619. [Online]. Available: https://www.mdpi.com/2071-1050/17/14/6619.

[13] S. Ebrahimi, T. Vahabzadeh, and J. Jatskevich, "Constant-parameter average-value model of power-electronic voltage-source converters with direct interface in electromagnetic transient simulators," *IEEE Open Journal of Power Electronics*, vol. 5, pp. 1446–1458, 2024. DOI: 10.1109/OJPEL.2024.3456729.

[14] L. Huang, C. Wu, D. Zhou, and F. Blaabjerg, "Impact of grid strength and impedance characteristics on the maximum power transfer capability of grid-connected inverters," *Applied Sciences*, vol. 11, no. 9, 2021, ISSN: 2076-3417. DOI: 10.3390/app11094288. [Online]. Available: https://www.mdpi.com/2076-3417/11/9/4288.

[15] B. Lennartson, *Reglerteknikens grunder*, 4. uppl. Lund: Studentlitteratur, 2002, ISBN: 9789144024165.

[16] R. A. Adams and C. Essex, *Calculus: a complete course*, eng, Ninth edition. 2018, ISBN: 9780134154367.

[17] H. Saadat, *Power system analysis*, eng, 3. ed. S.l.: PSA Publishing, 2010, ISBN: 9780984543809.

[18] *Snabb frekvensreserv (FFR)*, sv, Oct. 2024. Accessed: Apr. 14, 2026. [Online]. Available: https://www.svk.se/aktorsportalen/bidra-med-reserver/om-olika-reserver/ffr/.

[19] ENTSO-E, *Technical Requirements for Fast Frequency Reserve Provision in the Nordic Synchronous Area - External document*, Brussels, Belgium. Accessed: Apr. 14, 2026. [Online]. Available: https://www.svk.se/4ab5d1/siteassets/english/stakeholder-portal/prequalification/technical-requirements-for-ffr-v1.1.pdf.

[20] L. Dacklin, "Dynamic FFR from wind power - from simulation to reality," eng, 2024. Accessed: Apr. 14, 2026. [Online]. Available: https://hdl.handle.net/20.500.12380/308044.

[21] D. e. a. Sun, "Research on frequency inertia response control strategy of scessdfig system considering variable wind speed," *The Journal of Engineering*, vol. 2019, no. 16, pp. 2995–3001, 2019. DOI: 10.1049/joe.2018.8504. [Online]. Available: https://doi.org/10.1049/joe.2018.8504.

[22] P. S. Kundur and O. P. Malik, *Power System Stability and Control, Second Edition* (McGraw-Hill's AccessEngineeringLibrary), eng, Second edition. New York, N.Y: McGraw Hill LLC, 2022, ISBN: 9781260473544.

[23] S. Dulal, M. Olama, N. L. Thotakura, and Y. Liu, "Inertia estimation for power grids: A review of methods, challenges, and future prospects," *Applied Energy*, vol. 407, p. 127 333, 2026, ISSN: 0306-2619. DOI: https://doi.org/10.1016/j.apenergy.2025.127333. [Online]. Available: https://www.sciencedirect.com/science/article/pii/S030626192502063X.

[24] B. Adkins and R. G. Harley, *The General Theory of Alternating Current Machines: Application to Practical Problems*, 1st. Boston, MA: Springer US, 1975, ISBN: 978-0-412-12080-0. DOI: 10.1007/978-94-009-5802-9. [Online]. Available: https://link.springer.com/book/10.1007/978-94-009-5802-9.

[25] R. Teodorescu, M. Liserre, and P. Rodriguez, "Grid synchronization in single-phase power converters," in *Grid Converters for Photovoltaic and Wind Power Systems*. 2007, pp. 43–91. DOI: 10.1002/9780470667057.ch4.

[26] L. Harnefors and H.-P. Nee, "Model-based current control of ac machines using the internal model control method," *IEEE Transactions on Industry Applications*, vol. 34, no. 1, pp. 133–141, 1998. DOI: 10.1109/28.658735.

[27] R. Keim. "Understanding transfer functions for low-pass filters." Accessed: 2026-04-16, All About Circuits. [Online]. Available: https://www.allaboutcircuits.com/technical-articles/understanding-transfer-functions-for-low-pass-filters/.

[28] S. W. Smith, *The Scientist and Engineer's Guide to Digital Signal Processing*. California Technical Publishing, 1997, ch. 15, Accessed: 2026-04-16. [Online]. Available: https://www.analog.com/media/en/technical-documentation/dsp-book/dsp_book_ch15.pdf.

[29] R. Keim. "Understanding the first-order high-pass filter transfer function." Accessed: 2026-04-16, All About Circuits. [Online]. Available: https://www.allaboutcircuits.com/technical-articles/understanding-the-first-order-high-pass-filter-transfer-function/.

[30] J. Gärd, "Trimning av lead och lag filter," DIVA Portal, Tech. Rep., 2004, Accessed: 2026-04-16. [Online]. Available: https://www.diva-portal.org/smash/get/diva2:582537/FULLTEXT01.pdf.

[31] Svenska kraftnät, *Tekniska villkor för förkvalificering och leverans av FCR*, Sundbyberg, Sverige. Accessed: Mar. 20, 2026. [Online]. Available: https://www.svk.se/4977ad/siteassets/aktorsportalen/bsp-och-brp/aktuella-avtal-bsp-och-brp/aktuella-avtal-bsp/3-tekniska-villkor-for-forkvalificering-och-leverans-av-fcr-5937-1.pdf.

[32] Regatron AG, *TC.ACS Regenerative AC Power Supply*, Product Specification Page, Regatron AG, Rorschach, Switzerland, 2024. [Online]. Available: https://www.regatron.com/programmable-ac-power/tc-acs/.

[33] dSPACE GmbH, *MicroLabBox II: Compact laboratory system for RCP and HIL applications*, Accessed: 2026-04-17, dSPACE GmbH, Paderborn, Germany, 2024. [Online]. Available: https://www.dspace.com/en/pub/home/products/hw/microlabbox-ii.cfm.

[34] M. Gustafsson and N. Krantz, "Voltage collapse in power systems: Analysis of component related phenomena using a power system model," Chalmers University of Technology, School of Electrical and Computer Engineering, Göteborg, Sweden, Technical Report 215, 1995.

[35] R. AG, *Even more flexibility with ac-4-quadrant tc.acs systems from regatron*, en-US, May 2025. Accessed: Feb. 20, 2026. [Online]. Available: https://www.regatron.com/news/ac-4-quadrant-tc-acs-systems.

[36] T. Olsen and N. Ito, *Implement an effective loop tuning strategy*, Accessed: 2026-05-03, 2013. [Online]. Available: %5Curl%7Bhttps://www.emerson.com/is/content/emerson/en/corporate/news-and-events/articles/documents/implement-an-effective-loop-tuning-strategy.pdf%7D.

[37] R. Kong, S. Sahoo, Y. Song, and F. Blaabjerg, "Damping control and improvement of grid-forming inverter from a wideband stability perspective," in *2025 IEEE Applied Power Electronics Conference and Exposition (APEC)*, 2025, pp. 696–702. DOI: 10.1109/APEC48143.2025.10977067.

[38] Svenska kraftnät, "Bilaga 6: Provning," Svenska kraftnät, Tech. Rep. Svk 2021/5426, 2023, Accessed: 2026-04-17. [Online]. Available: https://www.svk.se/49b5e9/siteassets/1.om-kraftsystemet/legalt-ramverk/eu-lagstiftning/anslutningskoder/bilaga-6-provning.pdf.

[39] Energimarknadsinspektionen, *Energimarknadsinspektionens föreskrifter om fastställande av generellt tillämpliga krav för nätanslutning av generatorer*, sv, Dec. 2018. Accessed: Feb. 20, 2026. [Online]. Available: https://ei.se/om-oss/publikationer/publikationer/foreskrifter-el/2018/foreskrift-eifs-20182.

[40] Tillquist, *LQT400 - Configurable multi-transducer with 2 analogue outputs - Tillquist Group AB*. Accessed: Apr. 29, 2026. [Online]. Available: https://www.tillquist.com/en/power-automation/discontinued-products-archive/lqt400-configurable-multi-transducer-with-2-analogue-outputs.

[41] L. Kutscher, E. Notté, and K. Anderson, "Child labour in the extraction of strategic raw materials: A review and risk assessment," *Green Health*, vol. 1, no. 2, 2025, ISSN: 3042-5832. DOI: 10.3390/greenhealth1020014. [Online]. Available: https://www.mdpi.com/3042-5832/1/2/14.

[42] A. Olabi et al., "Renewable energy systems: Comparisons, challenges and barriers, sustainability indicators, and the contribution to un sustainable development goals," *International Journal of Thermofluids*, vol. 20, p. 100 498, 2023, ISSN: 2666-2027. DOI: https://doi.org/10.1016/j.ijft.2023.100498. [Online]. Available: https://www.sciencedirect.com/science/article/pii/S2666202723002136.

[43] B. Kennedy and E. Kikuchi, "Americans' shifting views on energy issues," Pew Research Center, Report, Apr. 2026. Accessed: May 10, 2026. [Online]. Available: https://www.pewresearch.org/science/2026/04/03/americans-shifting-views-on-energy-issues/.

DEPARTMENT OF ELECTRICAL ENGINEERING
CHALMERS UNIVERSITY OF TECHNOLOGY
Gothenburg, Sweden
www.chalmers.se

CHALMERS
UNIVERSITY OF TECHNOLOGY